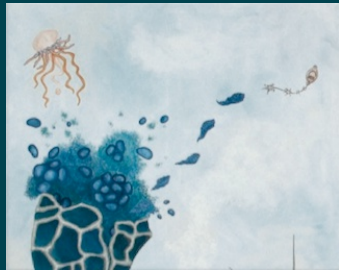


Late Breaking Proceedings of the European Conference on Artificial Life 2015



edited by
**Paul Andrews, Leo Caves, René Doursat,
Simon Hickinbotham, Fiona Polack,
Susan Stepney, Tim Taylor and Jon Timmis**

Late-Breaking Proceedings of the European Conference on Artificial Life 2015

ECAL 2015

Edited by:

Paul Andrews, Leo Caves, René Doursat, Simon Hickenbotham,
Fiona Polack, Susan Stepney, Tim Taylor and Jon Timmis



This work is licensed under the Creative Commons Attribution-NonCommercial-NoDerivs 3.0 Unported License. To view a copy of this license, visit <http://creativecommons.org/licenses/by-nc-nd/3.0/> or send a letter to Creative Commons, PO Box 1866, Mountain View, CA 94042, USA.

Table of Contents

Logical gates by glider-gun dynamics – the X-rule	1
<i>Andrew Wuensche, José Manuel Gómez Soto</i>	
Pedestrian Behavior Mining from Data	4
<i>Juan Galán-Páez, Joaquín Borrego-Díaz</i>	
Shaping the body to shape the behavior: a more active role of the morphology in the brain-body trade-off	7
<i>Francesco Corucci, Marcello Calisti, Helmut Hauser, Cecilia Laschi</i>	
Multi-level evolution, differential gene mobility, and the persistence of population diversity	9
<i>B. van Dijk, P. Hogeweg</i>	
Engineering Artificial Extraterrestrial Life?	12
<i>Alex Ellery</i>	
Thresholding Urban Connectivity by Local Connected Fractal Dimensions and Lacunarity Analyses	15
<i>Bashar Swaid, Eleonora Bilotta, Pietro Pantano, Roberta Lucente</i>	
Open-ended evolution in a web system	17
<i>Mizuki Oka, Yasuhiro Hashimoto, Takashi Ikegami</i>	
Maze Navigation and Memory with Physical Reservoir Computers	19
<i>Chris Johnson, Andrew Philippides, Philip Husbands</i>	
An unexpected discrepancy in a well-known problem: Kraskov estimators applied to spiking neural networks	22
<i>Pedro A.M. Mediano, Murray Shanahan</i>	
Analysis of causality network from interactions between nonlinear oscillator networks and musculoskeletal system	25
<i>Jihoon Park, Hiroki Mori, Asada Minoru</i>	
Simulated Robotic Autonomous Agents with Motion Evolution	27
<i>Neil Vaughan</i>	
Reaction-Diffusion Risk: Chemical Signaling in a Conquest Game	29
<i>Nathanaël Aubert-Kato, Olaf Witkowski</i>	
Author Index	31


Logical gates by glider-gun dynamics – the X-rule

Andrew Wuensche¹ and José Manuel Gómez Soto²

¹Discrete Dynamics Lab, London, UK, <http://www.ddlab.org>

² Universidad Autónoma de Zacatecas, Unidad Académica de Matemáticas. Zacatecas, Zac. México
andy@ddlab.org, jmgomezuaam@gmail.com

Introduction

This is a very brief overview of our recent paper (Gomez-Soto and Wuensche, 2015) about a new Life-like Cellular Automata (CA), the X-rule – a 2d, binary CA with a Moore neighborhood  and a λ parameter analogous to the game-of-Life (Berlekamp et al., 1982, Chapter 25), but not based on birth/survival and not fully isotropic. Glider-guns based on periodic oscillations between stable barriers were constructed, and interactions combining multiple glider-guns and eaters/reflectors were arranged and synchronised precisely to create the logical gates NOT, AND, OR and NOR required for logic universality, and potentially universality in the Turing sense, though this will require further work.

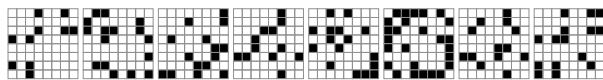


Figure 1: The rule-table of the X-rule – 512 neighborhood outputs are shown in descending order of their values, from left to right, then in successive rows from the top.

Glider-guns

The X-rule's glider-guns are analogous to Gosper's in the game-of-Life (Berlekamp et al., 1982, Chapter 25), but different in that they are constructed from a kit of parts, gliders and reflectors, that can be put together in many combinations to produce periodic oscillators based on bouncing/reflecting behaviour – pairs of gliders bouncing against each other and trapped between reflectors from which other glider types are ejected at periodic intervals.

This was achieved by introducing specific non-isotropic outputs within an isotropic precursor rule. Increasing the gap between reflectors increases the glider-gun period and reduces glider ejection frequency. These and other emergent structures enable flexible and versatile computational dynamics. Snapshots of the two basic glider-guns, GGa and GGb, are shown in figures 2 and 3, and figure 6 and 7 show the compound glider-gun GGc. So far GGa and GGc have provided the components for logic circuits.

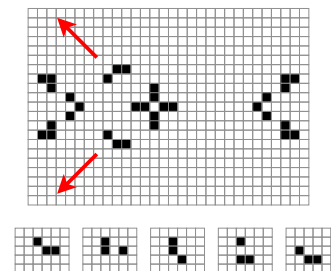


Figure 2: Basic glider-gun GGa shooting gliders Ga SW and NW, speed= $c/4$. The SE and NE directions requires a compound glider-gun (figure 6). *Inset*: the 4 phases of Ga SW.

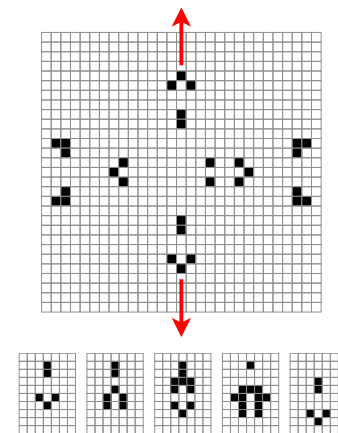


Figure 3: Basic glider-gun GGb shooting gliders Gb North and South, speed= $c/2$. *Inset*: the 4 phases of Gb South.

Searching for promising rules

The initially step was to search rule-space for emergent gliders and stable structure (eaters/reflectors) using the variability of input-entropy (Gomez-Soto and Wuensche, 2015; Wuensche, 2011, 1999) in figure 4. The search was restricted to isotropic rules only – equal outputs for any neighborhood rotation, reflection, or vertical flip – where rule-space is reduced to 2^{102} . The λ parameter (density of 1s) was also restricted to be similar to the game-of-Life. From a large rule sample, a shortlist of about 70 rules with both

gliders and stable structures were identified in the ordered sector of figure 4. Five rules, with gliders travelling both orthogonally and diagonally, were selected for further study.

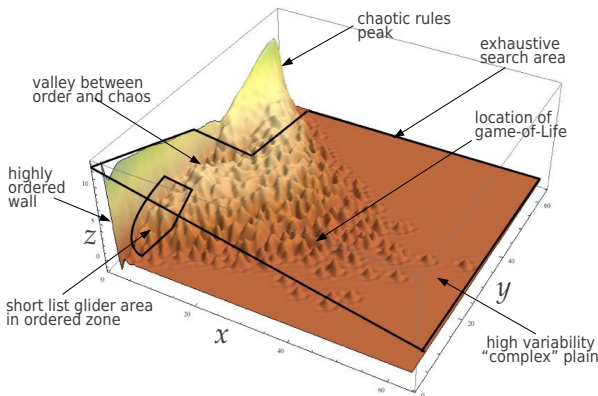


Figure 4: A scatter/frequency-plot (Gomez-Soto and Wuensche, 2015) of a sample of 93000+ rules. Min-max input-entropy variability x is plotted against mean entropy y , and (log) frequency (z) of rules on a 256x256 grid, which separates rule-space into fuzzy zones of chaos, order, and complexity. Promising rules were found in the ordered zone.

Constructing a reflecting/bouncing oscillator

The pivotal step in the project was to construct glider-guns based on simpler periodic oscillators. This involved building a periodic bouncing-colliding structure. From the short-list of five isotropic rules, we selected a rule, the X-rule precursor, with bouncing/reflecting behavior from spontaneously emergent objects: gliders G_a moving diagonally with speed= $c/4$, gliders G_c moving orthogonally with speed= $c/2$ (c is the speed of light), and three types of simple eaters/reflectors, (and rotations) 1 2 3. From G_c gliders and the eaters/reflectors we were able to construct the reflecting/bouncing oscillator in figure 5 where the distance between reflectors could be varied.

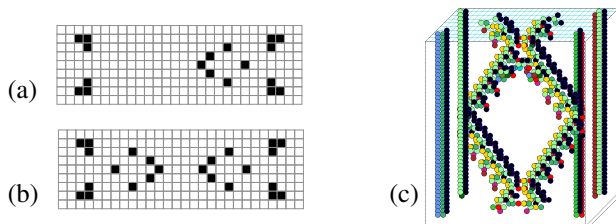


Figure 5: (a) A G_c glider bouncing back and forth between two reflectors. (b) A reflecting/bouncing oscillator (RBO) – two G_c gliders reflecting and bouncing off each other, gap=20, period=30 – as yet no gliders are ejected. (c) a representation of RBO showing 2D time-steps.

Creating glider-guns – the X-rule

Our strategy for creating glider-guns was to mutate outputs in the X-rule precursor’s rule-table with no restriction

on preserving isotropy, but retaining the essence of reflecting/bouncing oscillators (RBOs) in figure 5, and crucially – ejecting gliders.

Using automatic methods for mutating and testing we obtained two different glider-guns (figures 2 and 3) in a rule later named the X-rule (figure 1). In the testing sequence other rules produced GG_a (but not GG_b) – we decided to focus on the X-rule because it supported two glider-guns, reasoning that two are better than one. The X-rule differs from its precursor by just 11 out of 512 neighborhood outputs – its dynamics gives the appearance of isotropy to a significant extent.

X-rule glider-guns have a special property in that the gap between reflectors can be enlarged from the minimum – 24 for GG_a and 23 for GG_b . Only increments of +4 are valid in each case to preserve the glider-gun, which increases the oscillation period and thus reduces the frequency of the resulting glider-stream.

Emergent structures in the X-rule universe

The X-rule conserves the two emergent glider types G_a and G_c , and the three eaters/reflectors 1 2 3 (and rotations) from its precursor. These emerge easily from a random initial seed because the eaters/reflectors and phase patterns of G_a are very simple, and G_c has a simple predecessor – the pattern G_c-p and its rotations. There are two more emergent gliders in the X-rule, G_b , an orthogonal glider moving only North and South with speed $c/2$ in 4 phases, and G_d , an orthogonal asymmetric glider moving only West and East with speed $c/2$ in 4 phases where the asymmetry alternates about a horizontal axis.

The outcome of glider-glider and glider-eater/reflector collisions is highly sensitive to collision phases, and the point and angle of impact. Gliders can self destruct, form stable structures, transform, combine, and bounce off at different angles. Eaters/reflectors can be destroyed or transformed. In order to create logical circuits a catalogue of the possible collisions and interactions is desirable, and a start was made in (Gomez-Soto and Wuensche, 2015).

Compound glider-guns

To date, a basic glider-gun for glider G_c has not been found, and the basic glider-guns are restricted to preferred directions because of non-isotropy. However, compound glider-guns for G_c and G_a allow any direction. These are constructed from two or more basic glider-guns and eaters/reflectors, positioned and synchronised precisely, making self-contained and sustainable multiple oscillating colliding compound structures. Figures 6 and 7 are snapshots of selected examples, shown on a 93×85 lattice. Gliders (and other mobile patterns) appear with green dynamic time-trails of 20 time-steps.

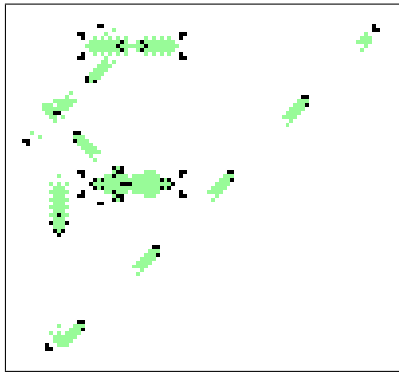


Figure 6: A compound glider-gun shooting Gc gliders towards the South, which bounce off a stable reflector to send Ga gliders NE.

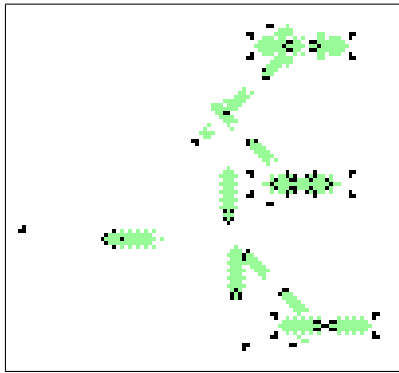


Figure 7: A compound glider-gun shooting Gc gliders towards the West made from a compound glider-gun shooting Gc gliders South, and a basic glider-gun below shooting Ga gliders NW.

Logical gates – logic universality

To demonstrate the X-rule’s logic universality we followed the game-of-Life method using glider-guns as “pulse generators”(Berlekamp et al., 1982, Chapter 25), to construct logical gates NOT, AND, OR, and finally the functionally complete NAND gate – a combination of NAND gates can implement any logic circuit.

In a glider-stream, the presence of a glider represents 1, and a gap 0. When two suitably synchronised glider-streams intersect, gliders either collide and self-destruct leaving a gap, or a glider passes through a gap and survives. Logical gates are implemented by combining perfectly spaced and synchronised input streams with intersecting glider-streams generated by one or more glider-guns.

All the gates in various orientations have been demonstrated (Gomez-Soto and Wuensche, 2015). As an example we show a NAND gate with the output directed NW.

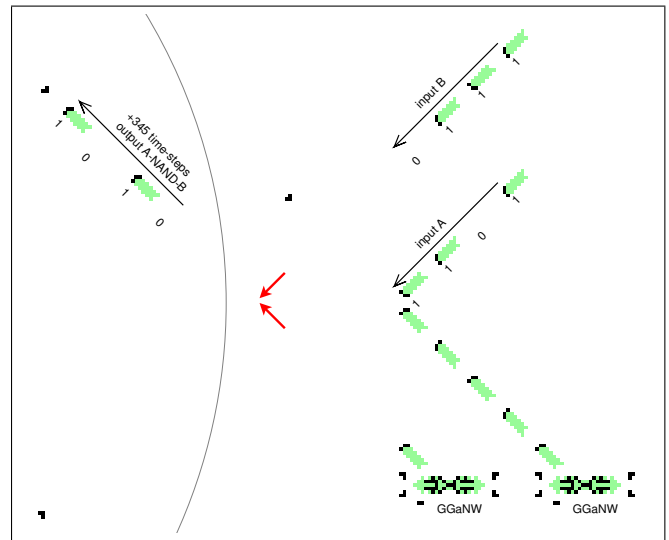


Figure 8: NAND gate: 1101 NAND 0111 giving the output 1010 heading NW. The first intersection is an AND gate, the second (at the red arrows) is a NOT gate.

Remarks

X-rule has underlying symmetry subject to marginal non-isotropy – the periodic oscillators based on reflecting/bouncing behaviour temporarily break symmetry to eject gliders. This is best perceived as dynamics, so the glider-guns, compound glider-guns, and logic-circuits will be shown in real time at ECAL15, using DDLab software.

Acknowledgements

Support was provided by DDLab and the Research Council of Zacatecas (COZCyT). We acknowledge DDLab software (Wuensche, 2011, 2015) for research and figures.

References

- Berlekamp, E., Conway, J., and Guy, R. (1982). *Winning Ways for Your Mathematical Plays*. Academic Press, New York.
- Gomez-Soto, J. and Wuensche, A. (2015). The X-rule: universal computation in a non-isotropic life-like cellular automaton. *JCA*, 10(3–4):261–294. preprint: <http://arxiv.org/abs/1504.01434/>.
- Wuensche, A. (1993–2015). Discrete dynamics lab (ddlab). <http://www.ddlab.org/>.
- Wuensche, A. (1999). Classifying cellular automata automatically. *Complexity*, 4(3):47–66. preprint: <http://uncomp.uwe.ac.uk/wuensche/downloads/papers/cplex.pdf>.
- Wuensche, A. (2011). *Exploring Discrete Dynamics*. Luniver Press. preprint: http://www.ddlab.org/download/dd_manual_2011/ExploringDiscreteDynamics.pdf.

Pedestrian Behavior Mining from Data*

Juan Galán-Páez and Joaquín Borrego-Díaz

Department of Computer Science and Artificial Intelligence – University of Seville, Seville, Spain
juangalan@us.es, jborrego@us.es

Abstract

A general -observation-based- qualitative framework to extract agent-based pedestrian behavior is presented. To extract qualitative rules from data we use tools, from Formal Concept Analysis, for implicational reasoning.

Introduction

Analysis of agent movement is a key research line in the study of (biological) complex systems. For example, the understanding the behavior of pedestrians is very important in urban design Guo and Huang (2008). This kind of problems has become an attractive field of study (see e.g. Helbing and Johansson (2014)). For example, in zones where pedestrian flow is dense, any small change in urban planning can have extreme consequences on pedestrian mobility. As it is stated in Canca et al. (2013), one of the most important goals in studies on pedestrian mobility and behavior is to evaluate the effect of new policies on pedestrian facilities before its implementation. A robust model to simulate pedestrian behavior is a good tool to prevent potential difficulties.

From the point of view of Artificial Intelligence, the pedestrian, as an agent, selects the next action from its own knowledge. Our thesis is that behavior has qualitative nature and is based on intuitive (geometrical, social, goal-driven) attributes. Thus it is interesting to explore how the reasoning with this kind of features can provide knowledge bases for modeling pedestrian behavior. The proposed methodology is based in both, Agent Based Modeling (ABM) and Formal Concept Analysis (FCA). In this work pedestrian behavior is considered individually by means of discrete ABM, where pedestrian flow emerges from interactions between pedestrians (agents) and the urban environment. The modeling is carried out from the pedestrian point of view in qualitative terms, allowing the use of reasoning and concept-mining methods in order to analyze pedestrian flow dynamics.

The aim of this paper is to show how to exploit knowledge extracted from observations (of real or artificial systems) to

study and explain -in a qualitative formalism- pedestrian behavior. The result of this process is, itself, a knowledge-based system. By using this system as a deliberative module for agents, we have implemented a general simulation framework for natural and artificial models of mobility.

Basic Agent-Based Model for pedestrians

In order to show how method works, consider as simulation environment an orthogonal grid where agents can make discrete movements. In each time step agents can move to any neighboring cell (Moore Neighborhood), where the chosen movements depends on local information agents obtain from their neighborhood and possibly additional information on urban planning. The environment consists of: **free cells** (any cell on which agents can move. In the basic model two agents cannot take up the same cell. Therefore, in the basic model, an occupied cell will be considered as an obstacle), **obstacles** (cells representing buildings, street furniture and other elements), and **exits** (representing possible pedestrians destination; these can be buildings/streets that are out of the area under study which are called *exits* as agents *leave* the simulation area through them).

The agent selects the best action (movement) according to their knowledge and the information he has about their neighborhood. To exemplify the general simulation framework, three basic agent behaviors will be considered: *best movement* (agent moves always to the adjacent cell closest to destination. This behavior can lead to blocked agents in certain scenarios.), *best movement with uncertainty* (agent makes the *best movement* with probability p or a random movement with probability $1 - p$), and *em any good movement*: (agent randomly moves to any of the adjacent cells toward destination. That is to say, any cell reducing agent's Manhattan distance to destination).

It is important to note that, due to spatial distribution within the environment, it is possible that the best movement in the short term (locally) will not be the best movement in the long term. The basic model can be improved in a number of ways: 1) Larger agents' range of vision (larger neighborhood). 2) Agents have memory. They can keep information of a number of past movements. 3) Agents have the ability

Partially supported by TIC-6064 Excellence project (*Junta Andaluca*) and TIN2013-41086-P t (Spanish Ministry of Economy and Competitiveness), cofinanced with FEDER funds

to communicate with and/or follow other agents. All these extensions can be added to the basic model by considering attributes specifying agents' new knowledge and abilities. However, the state description of an agent would be more complex and this could complicate the analysis of simulation results and the extraction of useful conclusions.

In order both to extract qualitative knowledge and to reason with this, **Formal Concept Analysis** (FCA) is used. This approach allows to extract and reasoning with knowledge from data. See Ganter and Wille (1997) and Aranda-Corral et al. (2013b) where details about the use of FCA to represent knowledge on cellular automata is presented.

Representing agent's knowledge. In the basic model the agent receives only information about the distance to its exit and neighboring obstacles. This first one is the *potential* of each cell with respect of agent destination, which evaluates the goodness of each possible movement of the agent, with respect to cells' distance to destination. In this regard, potential can be positive (the cell is closer to destination), negative (the cell is farther) or neutral. If any of the cells is an obstacle, it will not be taken into account in agent's decision.

In order to validate the proposal, experiments using two of the basic ABM for pedestrians (Best movement and Any good movement) have been carried out. Due to space limitations it has not been possible to consider more elaborate models on this article. Likewise two different attribute sets, based on cells' potentials, will be used as agents' (local) knowledge representation¹:

Detailed potentials (58 attributes): These estimate how good the potential of each neighboring cell is. Despite the potential being an abstract concept, in this case, it is based only on agents' distance till destination, for example to quantify potentials in terms of cell's *Manhattan distance* till destination.

Attributes *Will-Move-To-XX(Target)* contains information on agent's next movement. These will be target attributes for the reasoning system for prediction, in which a model is built from past information on agents' behavior.

Simplified potentials (42 attributes): This set provides information only on whether potentials are positive, negative or neutral without quantifying how positive or negative they are. The rest of attributes are the same in both attribute sets.

In both attribute sets, each (neighboring) cell is identified by its relative position with respect to the agent (that is to say, $\{TL, TC, TR, CL, CR, BL, BC, BR\}$). For instance *TL* refers to top-left cell, *CR* refers to center-right cell and *BC* refers to bottom-center cell.

Contextual selection for pedestrians

The reasoning system from Aranda-Corral et al. (2013b) allows the use of FCA-based tools for carrying out pedestrian

¹Standard qualitative attributes have been selected to show the method. The attribute selection can be expanded by adding any (computable) attribute the observer finds relevant

behavior simulations. From a contextual selection (formal context) it is possible to extract a knowledge base to be used by the reasoning system. The **contextual selection** contains information items similar (based on its context, that is, time, space and other properties) to the ones under study. Thus reasoning with this selection will provide more reliable entailment. For instance, let *a* be a pedestrian whose current position is known. Contextual selection to predict the next movement of *a* consists of:

Spatial dimension: Depending on the nature of the scenario under study it is possible to consider the whole pedestrian set or a pedestrian subset containing only those pedestrians closer to *a* (for big or heterogeneous scenarios), for instance, those pedestrians located in the same street as *a*.

Temporal dimension: A contextual selection for pedestrian dynamics usually contains information of agents' movements for more than one past time step. In order to estimate the next movement of a pedestrian *a* in a time step *T* the contextual selection for *a* in *T* will consist on other pedestrian movements in a recent time period of length *W*. In this way, the time window considered for the contextual selection would be $[T - W, T)$.

Attribute selection: Since different attribute sets can be used, for each setting the attribute set most suitable to be used as knowledge representation for *a* and its environment would be selected. In this concrete case (the pedestrian basic model), one of the two proposed attribute sets will be selected. In more complex scenarios the attribute set can include other attributes specific for the environment where *a* is located (spatial, temporal or from other nature).

FCA-based simulation of pedestrian flow

The process for computing the next movement, in a certain time step *M*, of a group of pedestrians for which past movements' information until a certain time step *N*, is known (where $N < M$), is as follows:

Stage 1: A formal context (the contextual selection) is built containing information on the *W* most recent time steps (movements) with respect to the target *M*. This formal context will contain, for each time step w_i and for each pedestrian, an object describing pedestrian's neighborhood at time step w_i and its next movement at time step (w_{i+1}) .

Stage 2: From this formal context, the knowledge base is extracted. According to the nature of the experiment, Stem basis or Luxenburger basis can be used.

Stage 3: In order to predict agent's next movement, a reasoning process is carried out. The initial facts consist of an attribute set describing agent's neighborhood at time *M*. The next movement at time step $M + 1$ is extracted from the entailment obtained by automated reasoning.

Soundness of the model. The standard way to specify (deterministic, reactive) agents includes $\langle S, T, Act, P, Do, acc \rangle$ with $Perceive : S \rightarrow T$, $Do : Act \times S \rightarrow S$ and $acc : T \mapsto Act$. Here *S* is the set

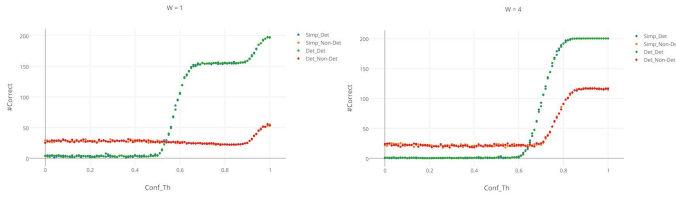


Figure 1: Results with different temporal windows

of states, T is a partition of S (due to perception features of the agent), Act is the actions set, and $Perceive, Do, acc$ are functions: P determines the agent state, Do determines the effect of an action on a state (reaching other state) and acc selects the action to be executed in a certain state. Agent execution from $\sigma(0)$ is the sequence $\{\sigma(t)\}_{t \in \mathbb{N}}$ where $\sigma(t+1) = Do(acc(Perceive(\sigma(t))), \sigma(t))$.

Given an attribute selection A , it is said that A is *descriptive* for the agent specification if each state of $t \in T$ can be interpreted as a set of attributes t^A of A , and for each $\alpha \in Act$ an attribute $\alpha^A \in A$.

Let S_n^K denote the subset of implications with positive support of the Stem basis for the context M_n^K which contains every observation of the history of the system from the initial state till the $\sigma(n)$ in $I_K = [-K, K] \times [-K, K] \subset \mathbb{Z}^2$ with a descriptive attribute set A . A distribution is a map $\Delta: \mathbb{Z}^2 \rightarrow \{agent, obstacle, free, exit\}$.

Lastly, denote by $s \in_{\Delta} X$, where $s \in T$ and $X \subset \mathbb{Z}^2$, the fact that there exists a cell c in X such that if an agent is located in $c \in \mathbb{Z}^2$ with the distribution $\Delta(X)$ then the agent perceives s . A distribution Δ is T -complete if $\{s : s \in_{\Delta} \Delta(\mathbb{Z}^2)\} = T$. A preliminary result on the soundness of the model can be stated as follows:

Theorem. 1. *Let Δ be a distribution and A be a finite descriptive attribute set for T (T finite). Suppose that Δ is T -complete and agents share the specification $\langle S, T, Act, P, Do, acc \rangle$. Then there exists $K > 0$ such that for all $n \in \mathbb{N}$*

$$acc(Perceive(\sigma(n)))^A \in S_n[Perceive(\sigma(n))^A]$$

Therefore the implication basis is sound to simulate agent behavior by means of a deliberative process. Note that the result does not give any estimation for $K = K(\Delta, acc)$.

Experiments and conclusions

In order to experiment with the methodology above described, a simulation platform has been developed. This consists of two modules, the first one comes with a NetLogo-based simulation viewer and is used for preliminary tests, and the second one focuses on computing massive simulations and is used for full experiments.

Due to the lack of space, only few of experiments (Fig. 1) are mentioned on a squared grid with 625 cells (25 per side) populated by 200 agents. In order to show the importance of the amount of information considered, results of

experiments for different window sizes W are provided (see Fig. 1, where $W = 1$ (left) and $W = 4$ (right)). Results of four different simulations are shown, one for each of the two possible knowledge representations (detailed or simplified) and one for each of the two possible pedestrian models (*best movement* or *any good movement*).

In each experiment a knowledge base is built from observable information in time steps $[T - W, T]$, and used (after selecting the implications with confidence greater than a certain threshold C_{th}) to predict agents' movement in time step $T + 1$. Results show the mean number of properly predicted movements. Each experiment is repeated for different values of the confidence threshold ($C_{th} = [0, 1]$) and $N = 100$ times for each value, in order to obtain a reliable estimate.

From experiments we can conclude that there is not substantial difference between the two representations used. It is worthy to note that a small uncertainty in agents' behavior (*any good movement*) leads to a great increase in the error. The reason is that a step-by-step performance evaluation is too strict for non-deterministic behaviors.

The work is based on a general hybrid approach to phenomenological reconstruction of Complex Systems (CS), using FCA as main tool for conceptual data mining (see Aranda-Corral et al. (2013a)). In Aranda-Corral et al. (2013b), the idea was applied to a classic CA (Conway's game of Life). The approach presented in this work specifies and implement a general method for movable agents. The key advantage of this method is that the observer can select (computable, qualitative) attributes in order to understand (and model) pedestrian behavior. The selection can comprise any feature on both, pedestrians and streets. From this selection, our method provides a qualitative model.

References

- Aranda-Corral, G. A., Borrego-Díaz, J., and Galán-Páez, J. (2013a). Complex concept lattices for simulating human prediction in sport. *J. Syst. Sci. and Complexity*, 26(1):117–136.
- Aranda-Corral, G. A., Borrego-Díaz, J., and Galán-Páez, J. (2013b). Qualitative reasoning on complex systems from observations. In *Hybrid AI Systems*, volume 8073 of *Lecture Notes in Computer Science*, pages 202–211. Springer.
- Canca, D., Zarzo, A., Algaba, E., and Barrena, E. (2013). Macroscopic attraction-based simulation of pedestrian mobility: A dynamic individual route-choice approach. *European J. Op. Res.*, 231(2):428 – 442.
- Ganter, B. and Wille, R. (1997). *Formal Concept Analysis: Mathematical Foundations*. Springer-Verlag New York, Inc., Secaucus, NJ, USA, 1st edition.
- Guo, R.-Y. and Huang, H.-J. (2008). A modified floor field cellular automata model for pedestrian evacuation simulation. *Journal of Physics A*, 41(38):385104.
- Helbing, D. and Johansson, A. (2014). Pedestrian, crowd, and evacuation dynamics. In Meyers, R. A., editor, *Encyclopedia of Complexity and Systems Science*, pages 1–28. Springer.

Shaping the body to shape the behavior: a more active role of the morphology in the brain-body trade-off

Francesco Corucci¹, Marcello Calisti¹, Helmut Hauser² and Cecilia Laschi¹

¹The BioRobotics Institute, Scuola Superiore Sant'Anna, Pisa, Italy

²Department of Engineering Mathematics, University of Bristol, Bristol, United Kingdom
Contact: f.corucci@sssup.it

Abstract

In recent years the concepts of embodiment and morphological computation brought an important paradigm shift in a number of research fields such as robotics, artificial intelligence, and artificial life. One of the most remarkable implications of these theoretical frameworks is the idea that the body has indeed an active role in the emergence of intelligent and adaptive behavior. It has been shown that in many cases it is possible to achieve complex behaviors with no "brain" at all (i.e. with no control – as in the case of passive dynamic walkers, or with a simple, periodic, open-loop control – as in the case of many walking and running robots). This view opens a number of intriguing questions, like: to what extent can we outsource intelligence to the body? What kind of behaviors can we achieve without introducing control? These questions fall under what is sometimes called the *brain-body trade-off*. With this abstract we aim at contributing to such a discussion by presenting some recent results of our work from an original perspective. The ultimate goal is to show that the body can have a more active role in achieving diverse behaviors. To stress this concept, we operate at one of the extremes of the brain-body continuum in which the role of the brain (or controller) is close to zero, i.e. the one of self-stabilizing robots with periodic open-loop control. There are many examples of such robots in robotics research, characterized by some common features. First, those robots have a morphology that is typically carefully engineered by human experts, often following heuristic design criteria and trial and error tests. This appears to be limiting if we consider the complexity of a robot's design space and the fact that such approaches are not able to explore many possibilities with respect to morphology and behavior. Second, although facilitating control, morphology usually has a *passive* role: once the design is fabricated morphology stays unchanged over the life span of the robot, and often operates in one or few, fixed, working regimes (or *attractors*, in a dynamical systems' view). Third, their behavioral diversity is usually limited, and where it is not the case, it is achieved by varying the controller, not by exploiting the morphology. Here we propose a systematic procedure that allows to design self-stabilizing robots exploiting the full potential of the morphology to achieve a diversity of behaviors. The key idea is to actively and dynamically involve the morphology in producing diverse behavior, resorting to the concept of *morphosis* or *morphing*, i.e. the possibility for a robot to control/experience a morphological change during its life span. The idea is to allow the robot to *change its shape to change its behavior*, in presence of a fixed controller: a walking robot may morph to switch to a running gait, while

an arm performing a limit cycle movement (e.g. exploration behavior) may morph to perform a reaching or a grasping movement. Given a basic morphological structure, an evolutionary process maximizing a metric of *behavioral novelty* is first ran to explore the space of morphology-enabled behaviors. This process allows to simulate a very large space of robot configurations without the restriction and the biases of the common trial and error, heuristic design procedures. Then an automated clustering procedure is executed to group the results of the evolutionary process into subsets of similar morphologies. Inside these clusters we search for functional robot configurations that are close in the morphology space, but far apart in the behavior space. Those configurations are selected as candidate morphologies to apply morphing, implemented as a gradual transition from one morphology to another: this way a slight morphological change can result in a macroscopic change in the behavior. In what follows some details regarding the procedure and the achieved results are provided. It is worth noting that there are considerable differences among this study and others in which novelty-based search is adopted to evolve morphologies (the closest one being Lehman and Stanley (2011b), where the focus is on combining the pressure towards novelty with the one towards performances). In addition to differences in the goals and in the applied methodology, the most notable, general, difference is that these works do not consider morphing, being instead the core of this work. For further details the interested reader is encouraged to refer to Corucci et al. (2015).

Case Study

The case study is the locomotion of the PoseiDRONE robot, an octopus-inspired soft-bodied underwater robot (Fig. 1a). The robot is composed of a central body, a floating module, and four compliant limbs. Each leg is actuated by a dedicated motor, whose control signal consists of a constant open-loop rotation. PoseiDRONE is an interesting case study for a number of reasons. First, it operates in water, where the body-environment dynamic coupling is stronger than in a terrestrial setting. In this setting a slight morphological change can result in a dramatic change in the behavior, which is desirable in order to experiment with morphing. Second, the robot morphology is simple enough to envisage a reconfiguration mechanism informed by the present results in future work.

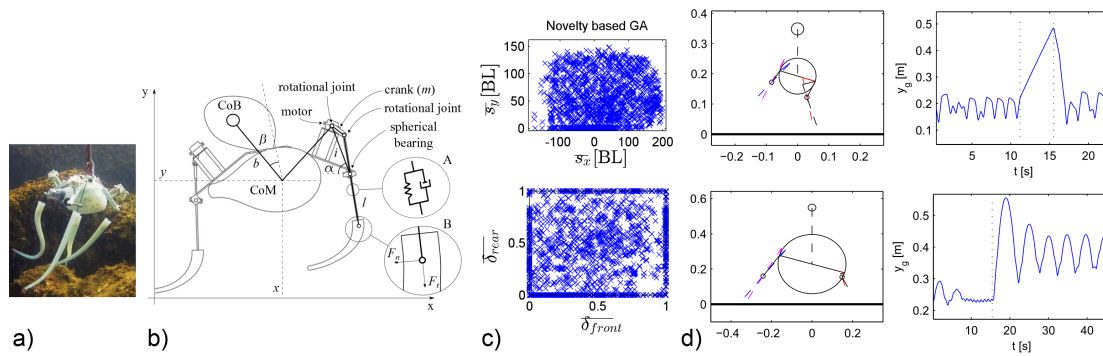


Figure 1: The PoseiDrone robot (a) and a schematic view of its model (b) (CoB stands for Center of Buoyancy, CoM stands for Center of Mass). c) Behavior space exploration: each cross represents the behavior of an individual of the final population. d) Example of two morphing robots selected by our procedure. Solid lines represent the CoM trajectory, while dashed ones identify morphing events. In the top row, the β parameter is morphed at $t = 11s$, entailing a transition from hopping to swimming. At $t = 15s$ β is brought back to its original value: the robot returns to its original gait. In the bottom row, the ratio between two geometrical parameters (m and i) is changed at $t = 15s$, entailing a transition from walking to hopping.

Methods

A dynamical model of the robot is adopted for this study (Fig.1b): the interested reader may refer to Calisti et al. (2014)). The model embeds a number of parameters, such as the one defining the geometry of the mechanism driving each leg, the dynamical properties of the legs (stiffness, damping, friction), the mean density of the robot, etc. A novelty-based evolutionary process appeared particularly suited to explore the space of morphology-enabled behaviors of the robot: the *novelty search* algorithm (Lehman and Stanley (2011a)) was thus adopted for this study, in combination with genetic algorithms (GAs). The algorithm is used to maximize novelty in a space of locomotion-specific behavioral features defined as $(\overline{s_x}, \overline{s_y}, \overline{\delta_{front}}, \overline{\delta_{rear}}) \in \mathbb{R}^4$, where $\overline{s_x}$ and $\overline{s_y}$ are, respectively, the normalized space traveled in the horizontal and vertical directions, and $\overline{\delta_{front}}$ and $\overline{\delta_{rear}}$ are the mean duty factors of front and rear legs (i.e. the percentage of time legs stay in contact with the ground). Model parameters are directly encoded into the genome. A methodology is then implemented to search inside the results of the evolutionary run (i.e. in the final population). Hierarchical clustering is applied in the morphology space to group similar morphologies. Then, inside each cluster, a search procedure is performed in order to find similar morphologies that maximally differ in terms of behavior (i.e. that are far apart in the behavior space defined by the features). Those morphologies are candidates for morphing, that is implemented as a feed-forward, gradual transformation from one morphology to another. The behavior of the robot is completely self-stabilizing, also during morphing.

Results and Conclusions

Results highlight that a novelty-based approach is indeed suitable to explore the space of morphology-enabled behav-

iors of a robot, producing a heterogeneous final population of functional robots in which it is possible to search for candidate morphologies for morphing (Fig.1c). Two morphing robots selected by our search procedure are presented (Fig.1d), in which a macroscopic change in the behavior is observable as a result of a slight morphological modification applied to just *one* parameter.

In this work we have pointed out that it is indeed possible to systematically exploit morphology to improve the behavioral diversity of a robot through morphing, leaving the control unchanged. The way this is done exploits the natural dynamics of the body and its self-stabilizing properties, in presence of a fixed control signal. In a dynamical systems view, instead of having the brain guiding the body towards different attractors, the body itself gains the freedom to shape the attractor landscape to change behavior. This entails a more active role of morphology, opening several intriguing possibilities for future research on embodiment, morphological computation, and adaptive behavior.

References

- Calisti, M., Corucci, F., Arienti, A., and Laschi, C. (2014). Bipedal walking of an octopus-inspired robot. In *Biomimetic and Biohybrid Systems*, pages 35–46. Springer.
- Corucci, F., Calisti, M., Hauser, H., and Laschi, C. (2015). Novelty-based evolutionary design of morphing underwater robots. In *Proceedings of the 2015 conference on Genetic and Evolutionary Computation (to appear)*. ACM.
- Lehman, J. and Stanley, K. O. (2011a). Abandoning objectives: Evolution through the search for novelty alone. *Evolutionary Computation*, 19(2):189–223.
- Lehman, J. and Stanley, K. O. (2011b). Evolving a diversity of virtual creatures through novelty search and local competition. In *Proceedings of the 13th annual conference on Genetic and Evolutionary Computation*, pages 211–218. ACM.

Multi-level evolution, differential gene mobility, and the persistence of population diversity

B. van Dijk and P. Hogeweg

Universiteit Utrecht, The Netherlands

b.vandijk@uu.nl, p.hogeweg@uu.nl

Only recently, the dominant role Horizontal Gene Transfer (HGT) in the evolution of prokaryotes is being recognized. Strikingly, HGT occurs orders of magnitudes more frequent than duplications, deletions, and even point mutations (Puigbo et al., 2014). This observation suggests an important role for gene-level selection for prokaryotic evolution, where novel adaptations can sweep a population on their own, while retaining background diversity (Shapiro et al., 2012). Related to this is the high diversity of antagonistic interactions even within single niches, despite the presence of isolates that are able to inhibit many other isolates (Vetsigian et al., 2011; Cordero et al., 2012). Inspired by the observation of mobile toxin genes in a background of ancestral resistance, and the surprising presence of “superkillers” in these diverse populations, we study a two-level eco-evolutionary model of prokaryotes undergoing HGT.

We model the evolution of HGT in a two-level spatial system (**Figure 1**). Bacteria compete for reproduction space by interacting by means of toxin and resistance genes. When bacteria die, the genes remain in the environment, and have a small chance to be taken up by living cells. Whether or not this DNA is integrated into the genome is a gene-dependent and evolvable feature. We focus our observations on the evolution of this GENE MOBILITY, and how this differs for toxin and resistance genes. As new genes flux into the eDNA plane only with very low frequencies, maintaining diversity is accomplished by cycling of the genes in the pan-genome.

Although initially both resistance and toxin genes evolve higher mobility, long-term evolution results in toxin genes that are much more mobile than resistance genes (**Figure 2**). High levels of resistance renders toxin genes rarely beneficial, favouring toxin genes that prolong survival by shifting selection towards the gene-level. Resistance genes are sufficiently selected on the level of individuals, and evolve low mobility in order to avoid the costly accumulation of redundant genes. Furthermore, after the

evolution of differential gene mobility, diversity is no longer decreasing (blue area). This suggests that the observed differential mobility is needed to maintain high diversity. Indeed, when the mobility of genes is set to equal values, all diversity is lost as toxin genes get extinct (data not shown). Despite frequent HGT, phylogeny adequately distincts the core-like resistance repertoires from the accessory toxin genes (**Figure 3**). Lastly, antagonistic interactions are only observed between the emergent core genomes, as has been previously observed for prokaryotes in soils and oceans (Cordero et al., 2012). In short, although our model only explicitly defines two levels of evolution, selection operates simultaneously at the gene level, the cell level, and the level of subpopulations with different core genomes. In contrast to ascribing diversification and evolution to clonal dynamics, multi-level evolution elegantly describes the observed dynamics of natural ecosystems. As an important contributor to multi-level evolution, we argue that HGT should get more attention in both biology and computer science.

Acknowledgements

This research was funded by the European Commission under FP7 grant no 610427.

References

- Cordero, O. X., Wildschutte, H., Kirkup, B., Proehl, S., Ngo, L., Hussain, F., Roux, F. L., Mincer, T., and Polz, M. F. (Sep 2012). Ecological populations of bacteria act as socially cohesive units of antibiotic production and resistance. *Science*, 337(6099):1228–1231.
- Puigbo, P., Lobkovsky, A. E., Kristensen, D. M., Wolf, Y. I., and Koonin, E. V. (2014). Genomes in turmoil: Quantification of genome dynamics in prokaryote supergenomes. *BMC biology*, 12(1):66.
- Shapiro, B. J., Friedman, J., Cordero, O. X., Preheim, S. P., Timberlake, S. C., Szabo, G., Polz, M. F., and Alm, E. J. (Apr 2012). Population genomic of early events in the ecological differentiation of bacteria. *Science*, 336(6077):48–51.
- Vetsigian, K., Jajoo, R., and Kishony, R. (Oct 2011). Structure and evolution of streptomyces interaction networks in soil and in silico. *PLoS Biol.*, 9(10):e1001184.

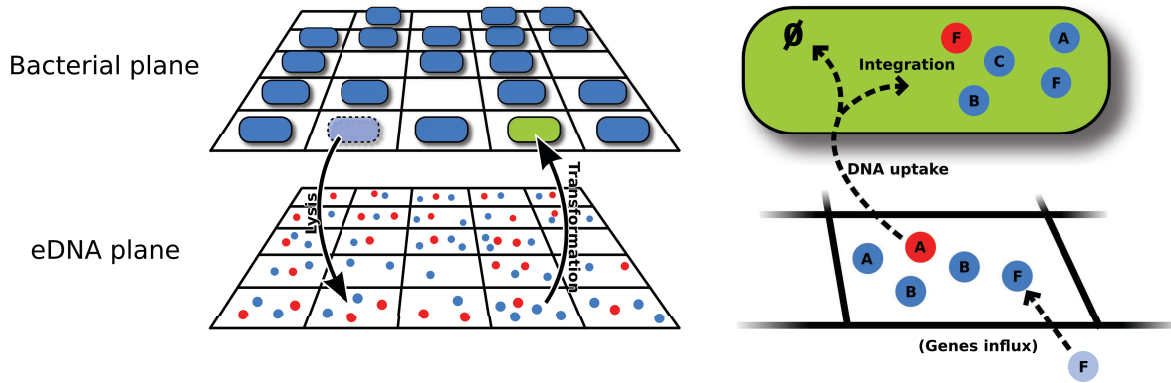


Figure 1: Graphical representation of the two-level model. Resistance genes are depicted as blue and the toxin genes as red. Genes can then be taken up with a fixed probability, and get incorporated with a probability that is evolved per gene. The eDNA diffuses and decays.

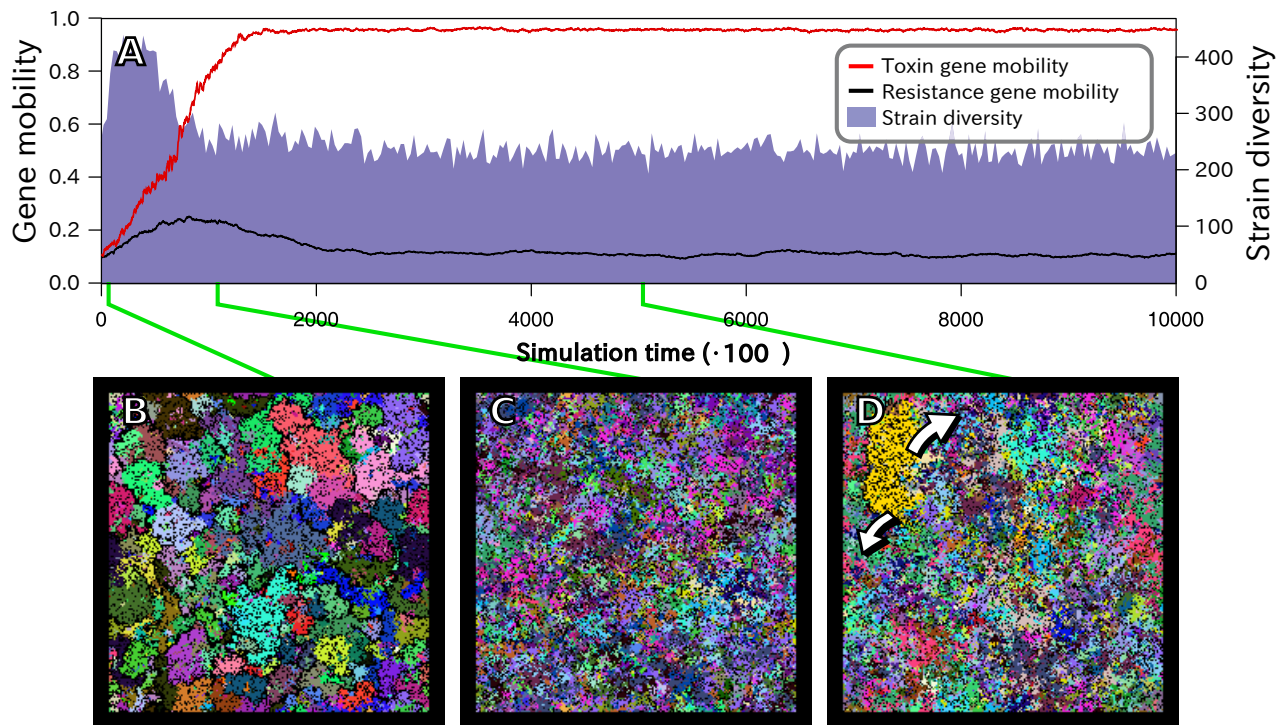


Figure 2: Evolution towards differential mobility for toxin and resistance genes. Average gene mobility for toxin and resistance genes (red and black line respectively), and strain diversity (blue area) is plotted against time. Panel A, B and C depict snapshots of the field-dynamics, where black depicts empty cells, and all other colours are unique strains.

Engineering Artificial Extraterrestrial Life?

Alex Ellery¹

¹Department of Mechanical & Aerospace Engineering, Carleton University, Ottawa, ON. K1S 5B6, Canada
aellery@mae.carleton.ca

Abstract

We present an outline of steps to engineer the physical embodiment of a universal constructor-based self-replicating machine. Given the centrality of self-replication to life, we offer some insights learned in our design of our universal constructor. Nevertheless, our self-replicating machine serves a practical purpose – to generate high productive capacity on the Moon at low-cost by exploiting its exponential population growth. The core of this machine is 3D printing technology that bears more than a passing resemblance to the universal Turing machine concept and the biological ribosome device. Our focus is on a fully functional end-to-end system capable of full self-replication. We present prototype components of our self-replicator concept.

The universal constructor concept conceived by John von Neumann (Burkes 1966) has only recently been simulated (Pesavento 1995). We have selected the Moon as our target environment due to its tectonic inertness, lack of environmental fluctuations and homogeneous geological properties. Furthermore, self-replication of productive capacity represents the only cost-effective approach for developing extraterrestrial resources (Freitas et al 1980; Chirikjian et al 2002). Our approach is to develop the basic components of a universal constructing self-replicator from the ground up rather than top-down to emulate (after a fashion) the process of the origin of life. The main problem has been to create sufficient functionality with a minimum of physical resources. Every component has a back-catalogue of processes and tools required for its manufacture. It is essential therefore to exploit simplicity, use multifunctional components, and use minimal materials to ensure material and parts closure. We present electric motors and vacuum tubes as multifunctional structures that enable a wide array of functions with a modest materials inventory.

The core of our self-replicating machine concept is the artificial ribosome – in this case, one or more 3D printers for layered manufacturing of metal, ceramic and plastic products from powdered feedstock material. There are several 3D printing technologies available that are differentiated by their printing heads – they offer general physical construction capabilities beyond that possible with subtractive manufacturing methods such as turning or milling. Our inspiration for the self-replicator is the RepRap, a fused deposition modelling 3D printer, that can print its own plastic parts (Jones et al 2001). To enable a RepRap-like 3D printer print a copy of itself, it would have to print in multiple materials – in principle, selective laser sintering can print

most materials while electron beam freeform fabrication can print metals. A laser would be challenging to incorporate into the self-replication process; an electron freeform fabricator however is essentially a high voltage electron gun in a vacuum tube. The self-replicator must be able to print its sensors, its motors, and its electronics. It was this sensorimotor aspect that was stressed in von Neumann's universal constructor through the constructing "robot" arm. The 3D printer is in fact merely a specific kinematic configuration of motors – a Cartesian robot. A reconfigurable robot can of course assume any specific kinematic configuration of motors according to its task (Yim et al 2007). It is these sensorimotor aspects that are our main concern but the control systems we are exploring are simple – we are avoiding any consideration of complex adaptive systems to explore the capabilities of simplicity.

The motor system is fundamental to any actuation capability as well as the 3D printer platform and printing head. Investigations into different motor concepts yielded our selection of traditional electromagnetic approaches but emphasizing simplicity of construction. Our universal electric motor design has been designed to be 3D printable. The motor core comprises alternating layers of silicon steel and plastic insulation which may be 3D printed and assembled in a hopper. Copper wire may be wound longitudinally using a spindle. The DC motor prototype functioned excellently and the core design is in the process of being 3D printed in both metal and plastic. Eventually, the stator magnets will be replaced by electromagnetic cores with a similar configuration as the rotor. A fully 3D-printable electric motor will demonstrate the viability of the self-replicator as the motor provides the basis for all other machines required (such as for surface finishing) – mechanisms, assembly grippers, grinders, lathes, mills, punches, conveyors, vehicles, drills, etc.

Our next consideration concerns the medium of control for our self-replicator – in our case, this is mediated through electronics. To eliminate reliance on solid-state electronics whose manufacture is complex, we propose vacuum tubes which possess relatively simple construction – heated cathode of tungsten with nickel conductors, metal control grid and metal anode plate encased in a glass tube. We have selected analogue neural networks as the fundamental unit of our control architecture given that it is Turing-complete (Siegelmann & Sontag 1995) and indeed may offer super-Turing capacities (Siegelmann 1995). We have built a modified Yamashida-Nakaruma analogue neuron constructed from an op-amp configuration (Yamashita & Nakaruma 2007). A two-neuron version has been demonstrated

controlling a desktop rover successfully implementing obstacle avoidance. We are currently investigating a means to implement online backpropagation learning in hardware. Task-specific neural networks offer a more compact physical footprint in vacuum tubes than attempting to construct a room-sized general purpose architecture. A 3D printer implementation thus constitutes a Turing machine that prints a specific neural network circuit for the task required according to its input program (be it punch cards or other storage medium).

Given that most sensory modalities (velocity, force, pressure, etc) are derivative from position sensors, potentiometers in conjunction with RCL circuitry offer feedback and general measurement capability. We have demonstrated that simple sensors in the wheels of a rover vehicle, in conjunction with neural net models, can provide online estimates of soil parameters as the rover traverses the soil (Cross et al 2013) – a useful capability for geotechnical surveying. Further sensors that may be readily manufactured include piezoelectric sensors (of quartz manufactured from lunar silica) and light sensors (of selenium mined in association with FeS deposits from iron meteorites).

Material feedstock for 3D printers must be mined from raw material, concentrated, and chemically processed – this goes beyond the von Neumann kinematic and cellular automata models. Such in-situ resource utilization is scheduled to be demonstrated with the Resource Prospector Mission (RPM) scheduled for launch to the Moon in 2018. The principle here is to minimize the elements that we extract. Lunar regolith is an unconsolidated inorganic soil representing a mixture of minerals and adsorbed volatiles. Lunar regolith may be readily scooped by rover such as a bucket wheel. One of the minerals in lunar regolith is ilmenite (FeTiO_3) that may be readily extracted magnetically. Ilmenite also concentrates volatiles hydrogen, helium and a number of carbon gases that may be extracted by heating ilmenite to $\sim 700^\circ\text{C}$ and then fractionally distilled. Further heating with hydrogen to $\sim 1000^\circ\text{C}$ decomposes ilmenite into evolved water, iron metal and titania ceramic. The water may be electrolyzed with the hydrogen recycled and oxygen stored. Titania is a useful ceramic that together with natural or manufactured lunar glass offers thermal and electrical insulation. Titania (and/or tungsten) may also be used for casting crucibles. Iron is a highly versatile metal that offers a range of alloys – wrought iron for tensile and compressive structures; tool steel (using tungsten) for cutting tools; electrical steel (using silicon) for high electrical resistance in motor cores; and kovar (using nickel and cobalt) for high conductivity electrical wiring and electrodes. Similarly, hydrogen and carbon compounds may be chemically processed with silica to yield silicone plastics that are both temperature and radiation resistant while minimizing consumption of scarce carbon sources. This provides flexible electrical insulation and oils for lubrication. The requirement for alloying materials – nickel, cobalt and tungsten (latter also for vacuum tubes) – requires iron meteorite sources (in near pure metal form). Mass concentrations detectable gravitationally mark the location of subsurface iron meteorite ores that will require drilling. We have explored the possibility of deploying bio-inspired drilling technology based on the wood-wasp ovipositor to minimize drilling infrastructure (Gao et al 2007). All the

chemical processes proposed involve only indigenous material with the exception of Na and Cl required as recyclable reagents. These must be imported from Earth but this provides a salt contingency to mitigate against replication proliferation.

All metabolic activity requires a source of energy – on the Moon, the self-replicator may exploit the most prodigious supply of energy, the Sun. Given that the majority of energy required will be thermal for material processing, Fresnel lenses can concentrate solar energy from 1360 W/m^2 to sufficient temperatures. Electrical energy may be generated through thermionic emission, commonly used in space nuclear reactors. It offers a practical conversion efficiency of $\sim 10\%$ superior to photovoltaic conversion in amorphous silicon. Thermionic emission is implemented through vacuum tubes. Electric motors provide the means for energy storage during the lunar night through flywheels.

We envisage our self-replicator to be self-contained within a regulated environment to minimize perturbations. This involves the use of automated manufacturing methods, site preparation and extensive jiggling but will still require some adaptability within limits. Nevertheless, the self-replicator will require effectors to acquire resources in an unstructured environment. This will involve rover vehicles for surface material acquisition and drills for subsurface material acquisition.

We have presented an overall architecture for a practical self-replicating machine. In addition, we have provided more detailed assessment of several component aspects – (i) 3D printable electric motor; (ii) hardware neural networks; (iii) geotechnic measurements; and (iv) biomimetic drilling. We suggest that this self-replicating machine does not constitute artificial life though it possesses most of its attributes. The traditional measurable properties of life (as defined for astrobiology missions) - self-replication, metabolic activity and self-encapsulation - are necessary but insufficient conditions for life. The key property of life is a history of information extraction from the environment and transmitting it onto subsequent generations, ie. a demonstrable evolutionary history (rather than the mere capacity to evolve which is implied by self-replication subject to the second law of thermodynamics). It is through the process of evolving a non-Markovian, non-commutative history that it demonstrates its autonomy as a living entity, ie. all living entities must be Darwin machines.

References

- Burkes A (1966) *Theory of Self-Reproducing Automata*, University of Illinois Press, Illinois
- Pesavento U (1995) Implementation of von Neumann self-reproducing machine. *Artif Life* 2 (4): 3370-354
- Freitas R and Gilbreath W (1980) *Advanced Automation for Space Missions*, NASA Conference Publication 2255, University of Santa Clara
- Chirikjian G, Zhou Y and Suthakorn J (2002) Self-replicating robots for lunar development. *IEEE/ASME Trans Mechatronics* 7 (4): 462-472
- Jones R, Haufe P, Sells E, Irvani P, Olliver V, Palmer C, Bowyer A (2001) RepRap – the replicating rapid prototype. *Robotica* 29 (1): 177-191
- Yim M et al (2007) Modular self-reconfigurable robot systems: challenges and opportunities for the future. *IEEE Rob & Autom Mag* (Mar): 43-52

- Siegelmann H & Sontag E (1995) On the computational power of neural nets. *J Comp & Sys Sci* 50: 132-150
- Siegelmann H (1995) "Computation beyond the Turing limit" *Sci* 268: 545-458
- Yamashita Y & Nakamura Y (2007) Neuron circuit model with smooth nonlinear output function. *Proc Int Symp Nonlinear Theor & App*, Vancouver, pages 11-14
- Cross M, Ellery A and Qadi A (2013) Estimating terrain parameters for a rigid wheeled rover using neural networks. *J Terramech* 50 (3): 165-174
- Gao Y, Ellery A, Vincent J, Eckersley S, Jaddou M (2007) Planetary micro-penetrator concept study with biomimetic drill and sampler design. *IEEE Trans Aero & Elect Sys* 43 (3): 875-88

Thresholding Urban Connectivity by Local Connected Fractal Dimensions and Lacunarity Analyses

Bashar Swaid¹, Eleonora Bilotta², Pietro Pantano², Roberta Lucente¹

¹ Department of Civil Engineering, University of Calabria, 87036 Rende (CS), Italy

² Department of Physics, University of Calabria, 87036 Rende (CS), Italy

swbasha@gmail.com, roberta.lucente@unical.it, bilotta@unical.it, pietro.pantano@unical.it

Abstract

The embodiment of fractal characteristics in the urban context relates to the mechanisms involved in the bio-functional evolution process and to the urban context's morphological characterization using fractal analysis. The failure of generalized fractal dimension to discriminate between active and non-active urban connections demands a precise method to estimate the local urban Connectivity. The focus of this research is on thresholding urban interactions, by multivariate discriminant function analysis based on Local Connected Fractal Dimensions and Lacunarity analyses. This invaluable local dimension analysis forms the core for estimating localized morphologic changes of different urban interactions levels, as a base for evolving fitness urban network by Genetic Algorithms.

The city's growth is guided by needs in local distribution and in communication among its parts (Courtat, Gloaguen, & Douady, 2011). These needs justify the complexity dimension investigations at localized level. According to Salingaros understanding the intricate connectivity of the living urban fabric it is necessary to undo the damage happened by erasing the fractal properties of the traditional city (A. Salingaros, 2005). This paper aims to thresholded Urban Connectivity Dimensions (U.C.D) using Fractal and Lacunarity logarithms by "FracLac" plugin in "ImageJ" software. The research chooses six cities (London, Paris, Rome, Milan, Aleppo and Cosenza) which represent diverse patterns in terms of U.C.D. Unfortunately, the *generalized box fractal dimension* (D) fails to differentiate successfully the morphological characterization found in different urban context. D is an overall or an average measure, and most of non-active and fragmented urban context show locally high-dimensional areas caused by nonfilling of the urban gaps together with locally low-dimensional areas caused by increased filling. The research has further investigated this problem using the concept of local connected fractal dimension.

Methods

The implemented methodology was applied to all case studies and involved two phases: maps digitization and fractal analysis.

Maps Digitization

The cities maps were elaborated by "Autocad" software and digitized as binary images in a computer with square pixels using "Xnconvert" software. The maps had a resolution of 1 pixel (1 pixel = 2 m), and consisted of 430 * 302 pixels.

Fractal Analysis

The computer program measured the total number of pixels local connected in a box of increasing size ϵ centered at a point x, y (Richard F. Voss, 1993). In this context, "local connected fractal dimension" relates to all the pixels within the largest box used for the analysis that belong to the cluster connected to the pixel on which the box is centered. This method was applied to all the pixels belonging to the urban context in the case studies. The scaling relation is found by the linear regression of the logarithm of the mass (pixels) in a box of size ϵ on the logarithm of ϵ . The relationship is expressed as: $\alpha = \log [M(\epsilon)] / \log (\epsilon)$. (1) Where $M(\epsilon)$ is the number of local connected pixels (eight-neighborhood connection) in a box of side size ϵ . The procedure is as follows: For every pixel that "belongs" to both urban connections and contexts in the cities (Gabriel Landini, 1995):

1. Call the current pixel P .

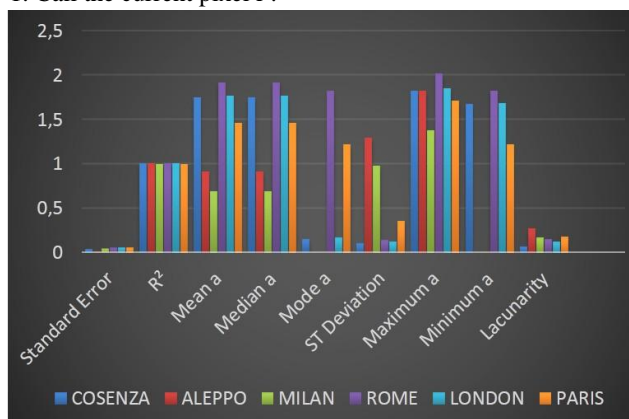


Figure 1: Summary of the parameters from local connected fractal dimension and Lacunarity analyses for the case studies.

- Find all the pixels connected to P within a 430 pixel-side window centered at P (this is the "local connected set" S).
- Count the number of pixels $M(\epsilon)$ of S , in boxes of increasing side size ϵ ($1 \leq \epsilon \leq 430$) centered at P .
- Calculate the local connected fractal dimension of S relative to P using equation 1 by linear regression of $\log(M(\epsilon))$ versus $\log(\epsilon)$.

Results

The methods were achieved by various analytical fractal dimension. Then the parameters from local connected fractal dimension and Lacunarity analyses were calculated and shown in Figure 1, which shows the mean values of the mean, median, mode, minimum, and maximum α and λ in the case studies, as well as the Standard Error and R2 (Coefficient Factor).

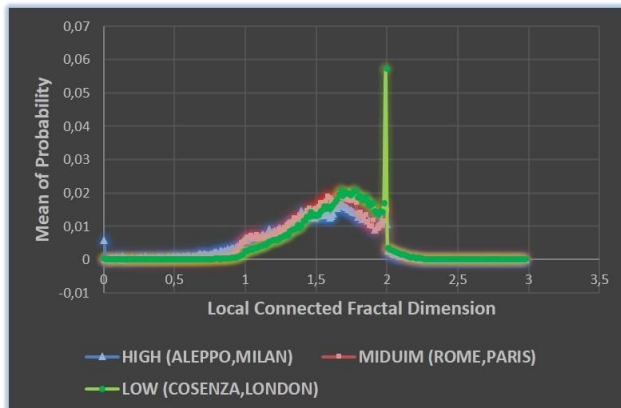


Figure 2: Mean distribution of the α value for the urban connectivity levels (high, medium and low).

Where none of the variables individually allowed a useful discrimination between the two groups. The mean distribution probability in the high, medium and low connectivity levels groups are shown in Figures 2. Note that the urban fragmented cases have a higher probability of high-dimensional features (near $\alpha \sim 1.7$ to 2.00 region) with large peak at 2 that corresponds to the areas devoid of urban interactions and connections (open spaces).

Multivariate Linear Discriminant Function Analysis

The mean values of the mean, mode α , and Lacunarity, were used in a multivariate linear discriminate function analysis implemented by "SPSS" software, to investigate any association that could lead to a classifier or univariate design (Huberty & Olejnik, 2006). Discriminate analysis successfully reclassified 6 of the 6 (100%) urban connections and contexts correctly in the original groups. This successfully of classification mean, mode α and Lacunarity emphasize their role as the main parameters controlling morphogenesis of urban connections. Producing a dimensional map is used due to interrelate every local connected fractal dimension with a single pixel figure 3. Which shows how the changes in structure and behavior of the urban interactions depend on the difference between the local connected fractal dimension and Lacunarity values (Bilotta & Pantano, 2006).

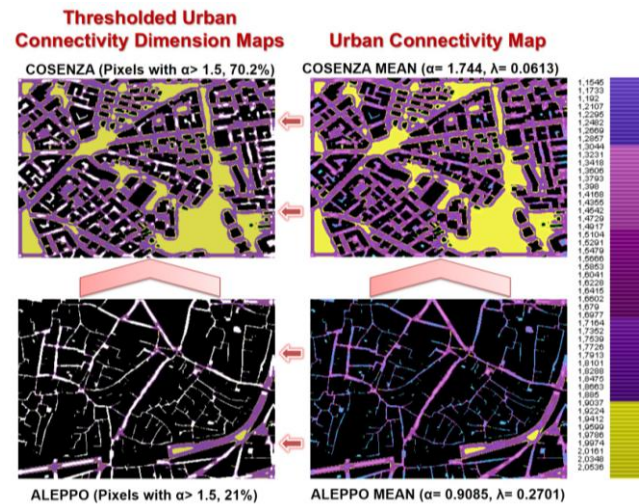


Figure 3: Urban connectivity in Cosenza and Aleppo cities and a thresholded version of the dimensional map showing only pixels with $\alpha > 1.5$.

The urban connectivity dimensional map represents a significant tool for evaluating and measuring the urban connectivity dimensions, which forms a real presenting of fractal criterion testing the cities geometry's as one condition for their success and a crucial guidance for the urban network's optimization process.

Conclusion

This morphological approach have been used to produce an objective method for assessment urban connectivity by a dimensional mapping, which was very successful for isolating areas with low connectivity dimension of high and medium ones. As well as helps to respond to the challenge for the contemporary city of how to superimpose competing connective networks in an optimal manner (Salingaros, 2004), by thresholding one of the essential characteristics in the cities "Network Interactions". Evolving an urban interactions adopting the new U.C.D threshold using genetic algorithms technique is under investigation.

References

- Bilotta, E., & Pietro, P. (2006). Structural and Functional Growth in Self-Reproducing cellular Automata. *Complexity*, 12-29.
- Courtat, T., Gloaguen, C., & Douady, S. (2011). Mathematics and Morphogenesis of the City, A Geometrical approach. *PHYSICAL REVIEW E*, 75-89.
- Gabriel Landini, P. I. (1995). Local Connected Fractal Dimensions and Lacunarity Analyses of 60° Fluorescein Angiograms. *Investigative Ophthalmology & Visual Science*, 49-55.
- Huberty, C. J., & Olejnik, S. (2006). *Applied MANOVA and Discriminant Analysis*. New Jersey: A JOHN WILEY & SONS, INC. PUBLICATION.
- Richard F. Voss, J. C. (1993). *Multifractals and the Local Connected Fractal Dimension*. *Applications of Fractals and Chaos*, 171-192.
- Salingaros, N. (2004). *Connecting the Fractal City*. PLANUM The European Journal of Planning, 1-27.
- Salingaros, N. (2005). *Principles of Urban Structure (Design/science/planning)*. Amsterdam: Tecne Press.

Open-ended evolution in a web system

Mizuki Oka¹, Yasuhiro Hashimoto¹ and Takashi Ikegami²

¹University of Tsukuba, Japan, ²The University of Tokyo, Japan
mizuki@cs.tsukuba.ac.jp

Abstract

By using an online photo sharing social network service called RoomClip, new aspects of open-ended evolution (OEE) in a web system are discussed. The reconstruction of a phylogenetic tree with relevant genotype-phenotype mappings is a necessary condition for discussing a Web system as an evolutionary system. By considering a photo as a phenotype and the annotated tags on the photo as genotypes, we found that OEE arises from innovative tags. Herein, we define innovation as the vitality of the service; it is triggered by the emergence of new tags that combine with many other tags. In other words, OEE can emerge as a progressive occurrence of such innovative tags. Based on our findings, we discuss the importance of genotype-phenotype mapping in deriving OEE.

Introduction

Evolutionary biology and its mathematical framework are widely used in various evolutionary analyses of nonbiological systems such as newsgroups, patents, languages, and food recipes. These systems have two properties in common; reconstruction of a phylogenetic tree with relevant genotype-phenotype mappings. For example, in case of US patent evolution (Chalmers et al., 2010), the emergence of a superstar patent (i.e., a patent that produces many other patents) was identified and characterized by measuring its term frequency-inverse document frequency (known as tf-idf).

Studies of nonbiological evolution have aimed to reveal the mechanism of open-ended evolution (OEE), one of the unsolved problems in artificial life studies (Bedau et al., 2000). OEE is defined as the continuous development of innovative technologies and functions found in a phylogeny of evolutionary systems (Chalmers et al., 2010). Thus far, we believe that OEE is found only in the evolution of life on Earth and in the technological evolution of mankind. In studying OEE, it is important to define and identify an *innovation* in an evolutionary system. In the case of US patents, innovative patents were identified by measuring the tf-idf and the number of citations by other patents.

In this study, we use an online social network service (called RoomClip) as an example to study OEE. RoomClip

is an online photo sharing service in which registered users post photos with tags. There exist follow-follower relations, and users can either 'like' or 'clip' posted photos (corresponding to retweet and favorite in Twitter, respectively).

We have access to the complete dataset from the launch of the service, and therefore, we can trace back all the relations created along the system's development. A genotype is considered equivalent to a set of tags and a photo, as the phenotype that is annotated by the set of tags. In this study, we define the system as showing OEE if it continues to create new tags, and we define innovation as the vitality (user activities) of a Web service system.

The main finding of this study is that OEE arises from tags that derive many co-occurrences with other tags, as a certain combination of tags invites more postings of photos, thus activating the entire service. As a result, new tags (or vocabularies) are created incrementally. We study the number of likes on photos by using the Hawkes process to look at the users' activation level. We show that the service becomes activated some time after the launch, and the activation level is maintained. We hope that our findings provide useful insights for studying the evolution of biological systems.

Analysis and Results

We used the data obtained from RoomClip (<http://roomclip.jp>), which was launched in April 2012. Since the launch of the service, the number of users has shown sustainable growth, and the total number of users is around 410,000, as of April 2015. For our analysis, we have gathered all of the posts, tags, likes, and clips as well as information on follow-follower relations for the period between April 2012 and April 2015.

Evidence of OEE: Continuous creation of new tags

In Fig. 1, we show the distribution of the distinct number of tags (vocabularies) over the number of annotations (Left) and the average number of tags used per photo over time (Right). It implies that the number of distinct tags is constantly increasing over time along with the number of tags used for each photo. New tags are constantly cre-

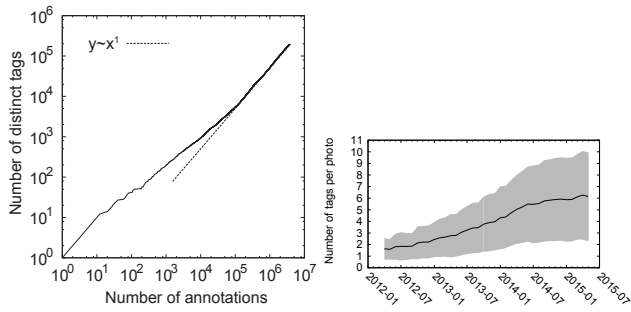


Figure 1: ((Left) Distribution of the distinct number of tags (vocabularies) over the number of annotations of the number of tags. (Right) Average number of tags used per photo over time.

ated (around 5% of tags are newly created on each posted photo), and more tags are used to characterize each photo as the service grows. It has been found that the Yule-Simon process (Simon, 1955) well describes the behaviour of the relation between the vocabulary growth and the number of annotations (Hashimoto et al., 2015).

Extraction of a phylogeny tree

We can extract a variety of phylogeny trees using the information available in the system, such as tags and photos. As one trial, we define the phylogeny between photos by the overlap ratio of the tag sets by the Jaccard coefficient (i.e., it is given by $A \cap B / A \cup B$ between a set of tags in photos A and B). The analysis reveals that evolutionary branching is accelerated by certain types of photos or a set of tags.

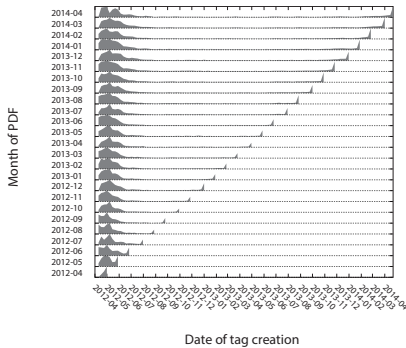


Figure 2: Histogram of used tags mapped to the time when they were created.

Co-occurrence of old and new tags

Fig. 2 shows a histogram of used tags mapped to the time when they were created. Both tags created at the early and most recent stages of the service are used frequently, and most of the others will become obsolete. This implies that the combination of old and new tags are used as a set in newly posted photos.

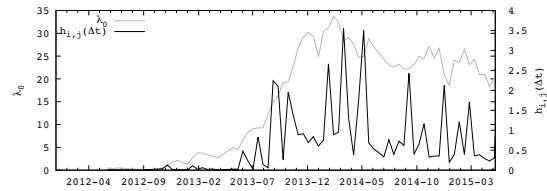


Figure 3: Time evolution of the default activity rate (gray line) and the responses from the inter-user network (black line) calculated by fitting to the Hawkes process.

Measuring the system's vitality

We measured the vitality of the service by using the Hawkes process, the equation of which is given as follows:

$$\lambda^k(t) = \lambda_0^k(t) + \sum_{k'} \int_0^\infty h^{k,k'}(t-\tau) \lambda^{k'}(t-\tau) d\tau,$$

where the first term describes the default activity rate and the second term, the inter-user network activity. In other words, $h^{k,k'}(t-\tau)$ expresses the contribution from user k' to user k with a time delay τ . We fitted the users time series of 'like' events by the Hawkes process by maximizing the likelihood and analysed the users those who posted more than 300 photos.

By using a general response function, we found that the integrated response function occasionally displays sharp bursts, as shown in Fig 3. The responses become bursty when the second part becomes dominant. This bursty nature became apparent after around July 2013.

Discussion

Our hypothesis here is that a Web system maintains its activity by increasing vocabularies in a progressive way. Certain types of tags stimulate users to invent new combinations. At the same time, users take photos to annotate with these tags. This type of tag, which we call innovative tags, can be used to derive the OEE of the service. As this study shows, we claim that genotype-phenotype mapping is a powerful mechanism to maintain and create the OEE, and it is applicable to other nonbiological and, possibly, to biological systems.

Acknowledgements

This work was supported by JSPS Grant-in-Aid for Scientific Research (C) Grant Number 15K00420.

References

Bedau, M. A., McCaskill, J. S., Packard, N. H., Rasmussen, S., Adami, C., Green, D. G., Ikegami, T., Kaneko, K., and Ray, T. S. (2000). Open problems in artificial life. *Artificial Life*, 6:363–376.

Chalmers, D. W., Francis, C. C., Pepper, N. M., and Bedau, M. A. (2010). High-content words in patent records reflect key innovations in the evolution of technology. In *Proceedings of the Twelfth International Conference on the Synthesis and Simulation of Living Systems, ALIFE 2010*, pages 838–845.

Hashimoto, Y., Sato, K., and Oka, M. (2015). Zipf's law and heaps' law in social tagging. *Proceedings of the 29th Annual Conference of the Japan Society of Artificial Intelligence*.

Simon, H. A. (1955). On a class of skew distribution functions. *Biometrika*, 42(3-4):425–440.

Maze Navigation and Memory with Physical Reservoir Computers

Chris Johnson¹, Andrew Philippides¹ and Philip Husbands¹

¹Centre for Computational Neuroscience and Robotics
University of Sussex
c.a.johnson@sussex.ac.uk

Abstract

The extent to which an organism's morphology may shape its behaviour is increasingly studied, but still not well understood (McGeer, 1990; Pfeifer and Bongard, 2007; Nakajima et al., 2015; Caluwaerts et al., 2012; Zhao et al., 2013). Hauser et al. (2011, 2012) introduced mass-spring-damper (MSD) reservoir networks as morphologically computing abstracted bodies. As these networks are abstracted from biological bodies, the two will share some properties and capabilities, and studying the former may give us useful clues about the latter. We have previously applied small MSD network pairs to the production of reactive behaviour often referred to as 'minimally cognitive' (Johnson et al., 2014, 2015). Here we go on to use similar controllers to solve a target-seeking problem for a mobile agent in a maze, which necessitates memory, over a finite but extended period. If MSD networks with relatively few elements but still high dynamic complexity can solve navigation problems requiring this kind of short term memory, then we may speculate that simple organisms can also.

MSD networks

In simulated MSD networks, point masses are connected by links which each consist of a spring and a damper in parallel (see Fig. (2)). In a true reservoir computing (RC) approach, the stiffness and damping coefficients of these elements, respectively, are randomised when the network is generated and do not change. Networks receive inputs in the form of forces applied to the point masses. The network forms a kernel, which projects its input streams into its higher-dimensional, and highly nonlinear, state space. In keeping with reservoir computing, the output from the network is a linear weighted sum of network states, and only these weights are trained.

Methods and Results

In an experiment based on that of Blynel and Floreano (2003), where a CTRNN controller was used, a group of 4 small MSD networks control a simulated ePuck robot which must navigate a T-maze and locate a target zone which is placed at the end of either the left or the right corridor (see Figures 1, 2 and 3). When the target is located, the robot is

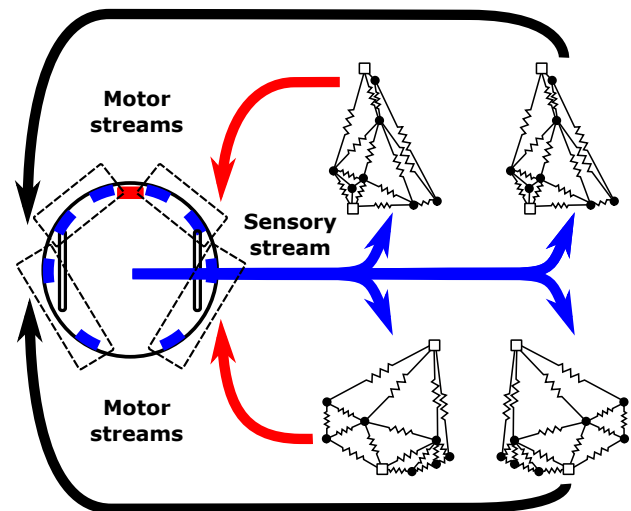


Figure 1: The ePuck and controller configuration. Camera (unused here) shown in red, on front of robot. Infrared (IR) distance sensors shown in blue. The rectangles with dashed outlines show how the sensors are grouped in pairs. Stimuli from paired sensors are summed before being input to the networks, so that the networks receive 5 inputs: 4 IR and one ground sensor to detect the target zone. The robot's wheels are shown as rounded open rectangles. Each of the robot's motors is controlled by an antagonistic pair of MSD networks. The back networks are identical to one another, but formed into a symmetric pair by connecting their inputs in reverse orders. In the case of the front networks, they are paired in the same way as the back ones, but symmetry is broken as they do not have the same weights as each other in the linear readout.

moved back to the start position and must navigate directly to the target zone, without searching other locations. In order to solve this problem, the robot must have memory of the target location at least until reaching the maze junction. Evolutionary methods are used to determine valid network parameters. In a break with the standard RC approach, stiffness and damping coefficients as well as readout weights

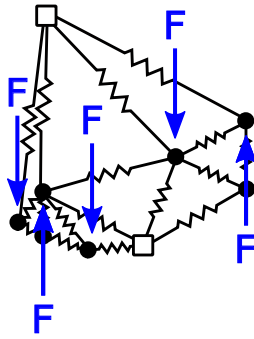


Figure 2: An MSD network from a valid controller. Square nodes are fixed, and round nodes move freely. Nodes are connected by links which consist of a parallel combination of spring and damper (dampers are omitted from this diagram for clarity). Inputs to the network are applied as forces on a subset of the free nodes. In this case, there are 9 nodes in total, and only 5 of the free 7 are driven.

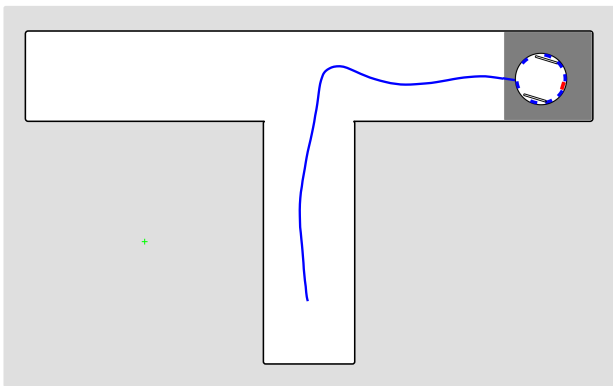


Figure 3: The ePuck in the T-maze. The target zone is shown in dark grey. In half of the evaluation trials, the target is on the right-hand side, as shown. In the other half it is on the left-hand side.

are evolved. The evolutionary algorithms and the MSD networks are implemented in the MATLAB IDE. The robot is simulated using the Enki 2D robot simulator C++ libraries (Magnenat et al., 2013).

Blynel and Floreano (2003) found that their CTRNNs stored the location of the target zone in the state of a network node. However, due to the ‘fading memory’ property, the MSD networks used here cannot store information indefinitely without the addition of a feedback loop (Hauser et al., 2012). In order to provide the possibility of memory in our controllers we added a feedback loop to a single network. Our first main discovery was that successful evolved controllers did not show signs of persistent memory. That being the case, we also tried evolving controllers without feedback loops. In both cases, it appears that transients in the network

responses to sensory input are surviving for approximately 45s (and perhaps longer), such that the robot makes the correct turn when it reaches the maze junction.

Conclusion

Without the addition of a feedback loop (Hauser et al., 2012), the MSD networks used here are limited by the ‘fading memory’ property. Practically, this means that the effect of any sensory input to the networks will have finite duration. To succeed in this target-seeking challenge, agents must have networks with dynamics rich enough to encompass quick response to sensors for steering and long-term transients for memory. The networks used here have been kept small to illustrate that networks with relatively simple structures can still exhibit complex dynamics which can be tuned by evolution to solve non-trivial behavioural problems. The linear readout of an MSD network can be interpreted as analogous to a primitive or peripheral nervous system. If these controllers can solve the problem of target-seeking navigation requiring short-term memory, then perhaps similarly primitive organisms can perform similar tasks.

Acknowledgements

Chris Johnson was funded by a University of Sussex graduate teaching assistantship.

References

- Blynel, J. and Floreano, D. (2003). Exploring the t-maze: Evolving learning-like robot behaviors using ctrnns. In *Applications of Evolutionary Computing*, pages 593–604. Springer, Berlin Heidelberg.
- Caluwaerts, K., D’Haene, M., Verstraeten, D., and Schrauwen, B. (2012). Locomotion without a brain: Physical reservoir computing in tensegrity structures. *Artificial Life*, 19(1):35–66.
- Hauser, H., Ijspeert, A. J., Fuchslin, R. M., Pfeifer, R., and Maass, W. (2011). Towards a theoretical foundation for morphological computation with compliant bodies. *Biological cybernetics*, 105(5-6):355–370.
- Hauser, H., Ijspeert, A. J., Fuchslin, R. M., Pfeifer, R., and Maass, W. (2012). The role of feedback in morphological computation with compliant bodies. *Biological cybernetics*, 106(10):595–613.
- Johnson, C., Philippides, A., and Husbands, P. (2014). Active shape discrimination with physical reservoir computers. In Sayama, H., Rieffel, J., Risi, S., Doursat, R., and Lipson, H., editors, *ALIFE 14: The Fourteenth Conference on the Synthesis and Simulation of Living Systems*, pages 176–183, Cambridge, MA. MIT Press.
- Johnson, C., Philippides, A., and Husbands, P. (2015). Active shape discrimination with compliant bodies as reservoir computers. *Artificial Life*. (in press).
- Magnenat, S., Waibel, M., and Beyeler, A. (2013). Enki - an open source fast 2d robot simulator (v1.0). <http://home.gna.org/>

enki/. stephane.magnenat@epfl.ch, markus.waibel@epfl.ch,
antoine.beyeler@epfl.ch.

McGeer, T. (1990). Passive dynamic walking. *The international journal of robotics research*, 9(2):62–82.

Nakajima, K., Hauser, H., Li, T., and Pfeifer, R. (2015). Information processing via physical soft body. *Scientific reports*, 5.

Pfeifer, R. and Bongard, J. (2007). *How the body shapes the way we think: a new view of intelligence*. MIT press.

Zhao, Q., Nakajima, K., Sumioka, H., Hauser, H., and Pfeifer, R. (2013). Spine dynamics as a computational resource in spine-driven quadruped locomotion. In *Intelligent Robots and Systems (IROS), 2013 IEEE/RSJ International Conference on*, pages 1445–1451. IEEE.

An unexpected discrepancy in a well-known problem: Kraskov estimators applied to spiking neural networks

Pedro A.M. Mediano and Murray Shanahan

Department of Computing, Imperial College London.
180 Queen's Gate, London SW7 2RH

pmediano@imperial.ac.uk ; m.shanahan@imperial.ac.uk

Abstract

While revisiting a problem in spiking neural networks (Shanahan, 2008) we discovered an interesting anomaly that we feel deserves further investigation as it could signify a useful contribution to the field of complex systems analysis. Robust methods for estimating information-theoretic measures like the two mutual information estimators in Kraskov et al. (2004) normally yield similar results, but we have found a case where they do not. Through extensive testing and the use of software libraries that are known to be reliable, we are confident that this seemingly contradictory outcome is not an error, and that it is a new discovery. We advocate the need for more thorough testing and benchmarking of estimators, and warn against the risks of drawing premature conclusions when using only one test method.

Introduction

The increasing availability of data and computational power are driving research in complex systems, notably in pioneering interdisciplinary fields like Artificial Life and Computational Biology. Therefore the study of complex systems has become even more vital. Reputable studies strengthen their claims using statistical analyses yet there is an inherent risk when using only one test method. This was highlighted beautifully in an Ig-Nobel-winning article that deliberately measured brain activity in a dead salmon (Bennett et al., 2011).

This vulnerability makes using multiple tests more appealing; perhaps the more the better. Naturally if the results differ between methods, this needs explaining. We have found a discrepancy in the outcome of the two current best-of-breed non-parametric estimators for information-theoretic measures introduced by Kraskov, Stögbauer and Grassberger (2004). This is interesting because the two estimators, known here as KSG 1 and 2, are almost equivalent — KSG 1 has higher bias, KSG 2 higher variance — and normally exhibit comparable behaviour (see Figure 1). Unexpectedly, the left-hand side of Figure 2 shows a peak in one line. This paper analyses and discusses this anomaly.

Methods

We discovered this anomaly when revisiting the problem of relating the dynamical complexity to the structural complex-

ity of spiking neural networks (Shanahan, 2008). An intriguing property of biological neural networks (brains) is their impressively rapid and seemingly paradoxical ability to produce a single coherent response despite small groups of neurons appearing to act individually in parallel. We therefore want to measure the equivalent behaviour in our system by seeing how it balances local and global information (in the general sense of the word). Reassuringly, this property can be measured independently from two diverse perspectives: network connectivity (which components connect to others) and network activity (how much traffic they send and receive). For our purposes, network activity equates to dynamical complexity and network connectivity to structural complexity. Understanding our assessment of these characteristics is helped if we first describe our system.

The system is a modular network of spiking neurons consisting of 8 modules of 100 excitatory neurons each. Each module has strong intra-connectivity and the inter-module coupling is achieved by adding long-range connections, the quantity of which is controlled by the parameter p which represents the fraction of long-range synapses between neurons in different modules. These 800 neurons are connected to a common pool of 200 inhibitory neurons so that the 8 clusters compete in a winner-take-all fashion. The model and parameter values for all neurons are from Izhikevich (2003), a well-established standard in the field. To sustain activity in the network, we supply every neuron strong Poisson-distributed current pulses with a rate parameter of 10 Hz.

We assess structural complexity using the small-world index S (Humphries and Gurney, 2008), calculated for the binary directed network formed by the 800 excitatory neurons. S quantifies the trade-off between high local clustering and short path length. We calculate all the relevant structural complexity measures using the Brain Connectivity Toolbox by Rubinov and Sporns (2010).

Similarly, we assess dynamical complexity using neural complexity C_N (Tononi et al., 1998). Neural complexity captures the balance between segregation and integration in a system by considering how the elements interact at all possible scales, from the smallest component up to the entire

system. This interaction is measured using mutual information, the building block of C_N , that in our experiments is directly estimated with either KSG 1 or 2.

We calculate all relevant information-theoretical measures using the free open source software package JIDT (Lizier, 2014). JIDT has been thoroughly validated against four other open implementations of KSG 1 and 2 so far. We use Kraskov et al.’s (2004) recommended setting $k = 4$, which is the default for JIDT.

We run the simulation for 200 s with a resolution of 1 ms. No measurements are recorded for the first 5 s to eliminate transient effects. The activity of the network is then recorded for 200 trials, measuring the firing rate of each cluster over a moving 50 ms window sampled at 20 ms intervals.

Results

We calculate S and C_N for every trial and show the relation between the two and the model parameter p in Figures 1–3. Figure 1 reveals a strong correlation between S and C_N ; therefore we conclude that dynamical complexity as measured by C_N is strongly correlated with structural complexity as measured by S . Figure 3 shows that S has a unique maximum at an intermediate value of the parameter p , indicating there is an optimal trade-off between high clustering and low path length. Figure 2 is more interesting to interpret and is the main focus of this paper.

In the mid- and high- p region, where the modular structure of the network is less pronounced, both KSG methods give similar results. This suggests that the neural complexity is smaller the more disordered the network.

In the low- p region, however, the methods yield qualitatively different results. The main difference between the two is that KSG 2 shows a peak in C_N at around $p = 0.05$, whereas KSG 1 displays monotonically decreasing behaviour.¹

Discussion

In this section we describe the validation process we have taken and discuss the reasons that lead us to believe this case represents a genuine discrepancy between the methods and not an error in our procedure. After extensive searching, we believe this to be a newly reported discovery.

It is known that the KSG estimators are slightly different, which becomes more apparent when dealing with smaller datasets: the smaller the dataset, the more you can expect a discrepancy, and the larger that discrepancy might be. Therefore it is vital to check that this difference is not merely a finite sample size effect. We test the effect of dimensionality and sample size by comparing both methods on synthetic data. We generate multivariate normal random samples of the same covariance, dimensionality and size as the

¹Note that $p = 0$ does not imply a fully disconnected network — the excitatory clusters still interact via the common inhibitory pool, despite having no direct excitation between them.

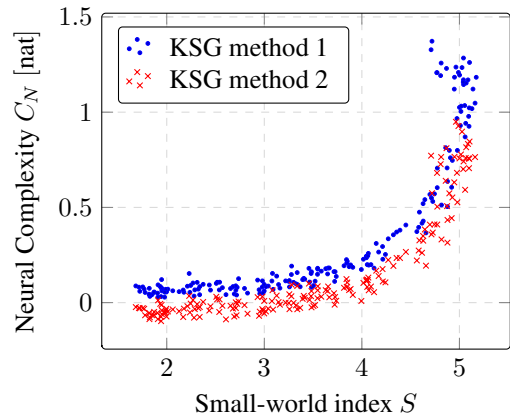


Figure 1: Neural complexity of the modular network calculated with both KSG estimators. When plotted against S , both methods show similar behaviour.

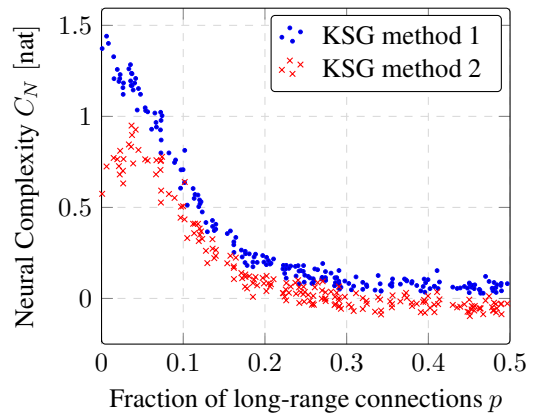


Figure 2: Neural complexity of the modular network calculated with both KSG estimators. When plotted against p , the methods show disagreement in the low- p region.

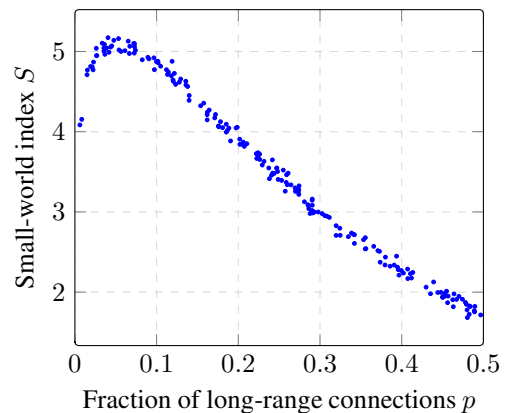


Figure 3: Small-world index of the modular network as a function of the fraction of long-range synapses p .

simulated data and apply both KSG 1 and 2. In this case, both methods show identical behaviour, with an average difference below 0.1%. Therefore, dimensionality and sample size are discarded as an explanation for the anomaly.

One plausible hypothesis is that the discrepancy is a consequence of some unknown bias that affects KSG 1 and 2 differently. To discard this possibility, we use several surrogate data testing methods to correct for different biases. Nevertheless the difference remains after applying any surrogate data method in our suite (Lucio et al., 2012). In fact, the results shown in Figures 1 and 2 are corrected using amplitude-adjusted Fourier transform. We conclude that this difference is more fundamental; or at least is not one that conventional surrogate data testing methods can correct for.

Another (unlikely) hypothesis is that these particular sampling choices are somehow pathological, and a different way of collecting the data would solve the problem. To test this, we apply different low- and highpass filters on the raw spike time series by changing the moving window size and step and by taking up to two time differences of the averaged data. Again, these procedures preserve the difference between the outcomes of both methods.

Finally, to verify that this is not an artifact of the factors that make up C_N , we use the same procedure to estimate other information-theoretic measures. For example, the same discrepancy still holds if we estimate simpler quantities — like the mutual information between any bipartition of the network — or other more involved quantities — like interaction complexity C_I , an approximation of C_N also introduced in Tononi et al. (1998).

Conclusions

KSG estimators, although generally accepted and broadly used in the analysis of complex systems, can yield inconsistent results when applied to more realistic cases that deviate from commonly used benchmarks.

The estimators produce qualitatively different results on our spiking neural network data, despite giving almost identical results when applied to an artificial dataset of the same size and dimensionality as the data extracted from the network. This difference is consistent and is obtained after both filtering the data and correcting the results using surrogate data methods.

This difference is important. An experimenter, Alice, using only KSG 2 to analyse her data will come to the conclusion that there is a peak of “interestingness” in a point where the network is not completely disconnected but still retains a strong modular structure; while her colleague Bob analysing the exact same data using only KSG 1 will conclude that the more segregated the network, the more complex behaviour is obtained. However, since both methods perform equally accurately in a common benchmark, there is no good reason to believe one of the two researchers is right while the other is wrong.

The benchmarks commonly used when testing estimators are helpful and necessary, but alone they are not sufficient to guarantee the validity of an estimator in other contexts. Real data on which the estimators are applied are often much less well-behaved than the synthetic data used in benchmarks. It is crucial to develop rigorous methods for testing, understanding and comparing estimators.

Acknowledgements

The authors gratefully acknowledge Brian Mitchell for his assistance with earlier versions of this document. This work is supported by an EPSRC doctoral training grant.

References

- Bennett, C., Baird, A., Miller, M., and Wolford, G. (2011). Neural Correlates of Interspecies Perspective Taking in the Post-Mortem Atlantic Salmon: An Argument For Proper Multiple Comparisons Correction. *Journal of Serendipitous and Unexpected Results*, 1:1 – 5.
- Humphries, M. D. and Gurney, K. (2008). Network ‘small-worldness’: a quantitative method for determining canonical network equivalence. *PLoS ONE*, 3(4):e0002051.
- Izhikevich, E. M. (2003). Simple model of spiking neurons. *IEEE transactions on neural networks / a publication of the IEEE Neural Networks Council*, 14(6):1569–72.
- Skarsvold, A., Stögbauer, H., and Grassberger, P. (2004). Estimating mutual information. *Physical Review E*, 69(6):066138.
- Lizier, J. T. (2014). JIDT: An Information-Theoretic Toolkit for Studying the Dynamics of Complex Systems. *Frontiers in Robotics and AI*, 1:37.
- Lucio, J. H., Valdés, R., and Rodríguez, L. R. (2012). Improvements to surrogate data methods for nonstationary time series. *Physical Review E*, 85(5):056202.
- Rubinov, M. and Sporns, O. (2010). Complex network measures of brain connectivity: uses and interpretations. *NeuroImage*, 52(3):1059–69.
- Shanahan, M. (2008). Dynamical complexity in small-world networks of spiking neurons. *Physical Review E*, 78(4):041924.
- Tononi, G., Edelman, G. M., and Sporns, O. (1998). Complexity and coherency: integrating information in the brain. *Trends in Cognitive Sciences*, 2(12):474–484.

Analysis of causality network from interactions between nonlinear oscillator networks and musculoskeletal system

Jihoon Park¹, Hiroki Mori¹ and Asada Minoru¹

¹Department of Adaptive Machine Systems, Graduate School of Engineering, Osaka University, Japan
jihoon.park@ams.eng.osaka-u.ac.jp

Introduction

In order to understand the interactions between the body, brain and environment that generate various behaviours, it is necessary to consider the network structure that dynamically emerges from interactions among the brain regions even though the brain has a fixed anatomical structure (Bullmore and Sporns, 2009). Kuniyoshi and Suzuki (2004) proposed a model in which adaptive behaviours emerge through body constraints as chaotic itinerancy that is induced by coupled chaotic elements. Moreover, Yamada and Kuniyoshi (2012) revealed the influence of embodiment in nervous system by embodied network. They constructed an embodied network using transfer entropy based on motor information and found that the embodied network had the properties of a complex network. However, they did not specify the structures of the network and dynamic changes in the network structure caused by different movements.

In this paper, we address the network structure relationship that dynamically emerges through interactions between the network, body and environment. We conducted a physical simulation using a snake-like robot with a nonlinear oscillator network (Mori et al., 2013) and estimated the network structure based on transfer entropy for each different movement. We defined a wired network for the physically embedded network and a causality network for the estimated network structure. In order to understand the relationships of the oscillators in the emergent casualty networks within the periodic behaviours by the robot, we extract the causality subnetworks by Infinite Relational Model (IRM) (Kemp et al., 2006) and analyze the networks by the complex network theory. Moreover, we measured average transfer entropy between body and network to know relationship between body and the causality networks.

Experiment and Results

We conducted a physical simulation with a network structure as shown in Figure 1. The network consisted of Bonhoeffer-van der Pol oscillator for output neurons and hidden neurons that directly and indirectly connect with muscles in the robot, respectively.

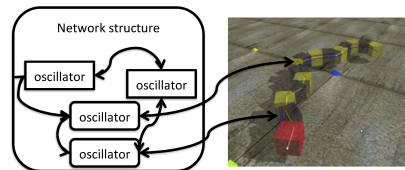


Figure 1: Model of snake-like robot

$$\tau \frac{dx}{dt} = c(x - \frac{1}{3}x^3 - y + z) + \delta(S_f - x) \quad (1)$$

$$\tau \frac{dy}{dt} = \frac{1}{c}(x - by + a) + \epsilon S_f \quad (2)$$

$$S_f = \begin{cases} \alpha I + (1 - \alpha) \frac{1}{K} \sum_{j=1, j \neq i}^N w_{ji} x_j & \text{if output neuron} \\ \frac{1}{K} \sum_{j=1, j \neq i}^N w_{ji} x_j & \text{else} \end{cases} \quad (3)$$

The oscillator neurons were updated according to Eqs.1 and 2. Each neuron was connected through binary-weighted connection of w , K is number of connections for each neuron. In these equations, a , b , and c control the neuron behaviour, z is a tonic input and δ and ϵ control the strength of the connections among the neurons. Moreover, α controls the strength of the ratio between the body and network, and I is the muscle length. In this research, we used $a = 0.7$, $b = 0.58$, $c = 2.0$, $\delta = 0.01$, $\epsilon = 0.01$, $\alpha = 0.5$ and $z = 0.3$. The network included 26 output neurons and 174 hidden neurons.

In order to distinguish different movements, Mean-shift clustering (Comaniciu and Meer, 2002) was used on a feature vector. The feature vector is constructed by correlation coefficient of between joint angles within a time window and dimensionally reduced by principal component analysis.

A causality network was constructed by means of transfer entropy (Schreiber, 2000) among the neurons for each longest movement pattern. The kernel estimation method was used to calculate the transfer entropy. Since transfer entropy has a direction, mutual information with IRM was used to estimate cluster and relationship in the causality network, here we defined each cluster as a subnetwork. The hyperparameters β and γ in (Kemp et al., 2006) were set 1 and

7. Figure 2 shows the topology of the wired network and the estimated relationships and clusters of the causality network according to the IRM with mutual information for the first and second longest movement pattern. As shown in Figure 2, causality networks when first longest movement pattern has less interaction with a subnetwork that has a many output neurons to another subnetwork.

In order to quantitatively measure interaction between body and network, average of transfer entropy was measured. As shown in Figure 3, low values of transfer entropy between hidden neurons and output neurons are observed during longer stable periodic movement.

To investigate the global property of the causality networks, average of clustering coefficient and shortest path length were calculated for each movement pattern. Figure 4 shows longer stable periodic movement when the causality network has a small clustering coefficient and large shortest path length that indicate the network has less complex network property.

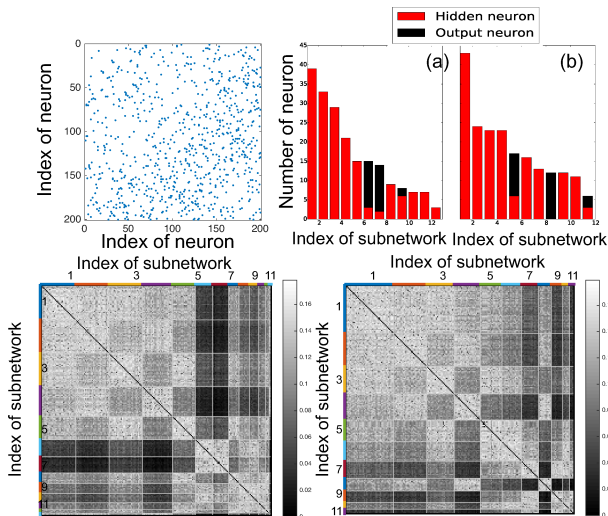


Figure 2: (top left) Topology of the wired network. (bottom left) Causality network for first longest movement pattern and (bottom right) second longest movement pattern are estimated by transfer entropy and clustered by IRM with mutual information. Colored bars on matrix indicate different subnetworks, and connections between different colored bars indicate interactions between subnetworks. (top right) Number of neurons including subnetworks for (a) first movement pattern and (b) second movement pattern.

Discussion and Conclusion

The presented results show that causality networks without complex network property and fewer interactions with subnetworks that had more output neurons to other subnetworks induced longer periodic movements. Therefore, periodic movement was dominated by the embodied network, and

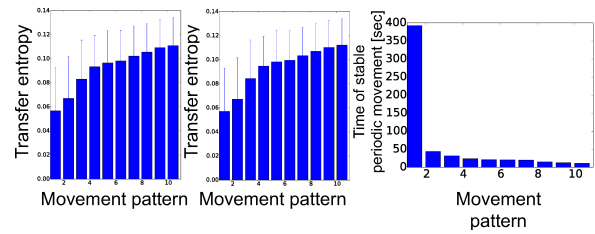


Figure 3: Average of transfer entropy (left) from hidden neurons to output neurons and (middle) from output neurons to hidden neurons. (right) Time of stable periodic movement for each longest movement pattern.

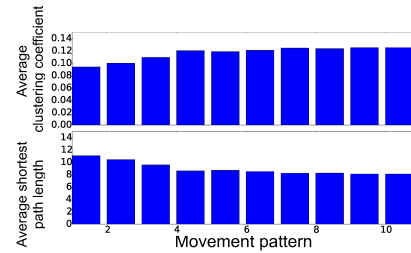


Figure 4: (top) Average clustering coefficient and (bottom) average shortest path length.

communication among the subnetworks induced exploratory movements.

Many issues require further study, especially the interactions with different body structure and wired network. The network structure also needs to be analysed by other property of complex network.

References

- Bullmore, E. and Sporns, O. (2009). Complex brain networks: graph theoretical analysis of structural and functional systems. *Nature Reviews Neuroscience*, 10(3):186–198.
- Comaniciu, D. and Meer, P. (2002). Mean shift: a robust approach toward feature space analysis. *Pattern Analysis and Machine Intelligence, IEEE Transactions on*, 24(5):603–619.
- Kemp, C., Tenenbaum, J. B., Griffiths, T. L., Yamada, T., and Ueda, N. (2006). Learning systems of concepts with an infinite relational model. In *Proceedings of the 21st National Conference on Artificial Intelligence - Volume 1, AAAI'06*, pages 381–388. AAAI Press.
- Kuniyoshi, Y. and Suzuki, S. (2004). Dynamic emergence and adaptation of behavior through embodiment as coupled chaotic field. In *IROS*, pages 2042–2049. IEEE.
- Mori, H., Okuyama, Y., and Asada, M. (2013). Emergence of diverse behaviors from interactions between nonlinear oscillator complex networks and a musculoskeletal system. *European Conference on Artificial Life 2013*, 12:324–331.
- Schreiber, T. (2000). Measuring information transfer. *Physical review letters*, 85(2):461–464.
- Yamada, Y. and Kuniyoshi, Y. (2012). Embodiment guides motor and spinal circuit development in vertebrate embryo and fetus. In *ICDL-EPIROB*, pages 1–6. IEEE.

Simulated Robotic Autonomous Agents with Motion Evolution

Neil Vaughan¹

¹Bournemouth University, Data Science Institute,
Talbot Campus, Fern Barrow, Poole, Dorset, BH12 5BB
nvaughan@bournemouth.ac.uk

Abstract

This research implemented autonomous control of robotic agents. The movement controls are simulated within a virtual environment. The control system algorithms were subjected to evolution. Genetic algorithms were implemented to enable the robotic agents to adapt in response to objects within the virtual environment. Additionally, each robot's physical characteristics were subjected to evolution through a survival of the fittest system based on crossover with random mutations. Survival of the fittest was simulated by a shortage of food causing competition. When the food quantity was increased the evolution rate decreased. With increased food, there was reduced competition and average fitness stopped increasing over time. Removing the food bottleneck stopped the survival of the fittest mechanism.

Introduction

The aim of artificial life is to exhibit characteristics of living organisms. Artificial life fits into three categories: (i) Microscopic systems such as chemical, cellular and tissues. (ii) Mesoscopic systems such as whole organisms. (iii) Macroscopic systems such as entire species and collective societal group (Bedau et al. 2003).

This research fits in category (ii) looking at the evolution of algorithms to control movement of a robotic autonomous agent. Also within category (iii) this research covers the group dynamic evolution by measuring changes in evolutionary rate within the group (species) of robots in a competitive environment and when bottlenecks are removed or reduced.

Types of Robotic Motion Control

Several recent research efforts have focussed on simulating evolution. Programs like Avida can model evolution of simulated organisms, made up of algorithms which reproduce. With Avida, organisms are represented as a string of commands which are executed. Programs like Avida can autonomously evolve basic computer software containing logic and comparison functions, for use in controlling physical robots. This digital evolution enables a fundamentally new approach to software design. Evolved program DNA can be cross-compiled into other languages and executed directly within physical robots or other systems. Avida was used to demonstrate that evolution can produce complex features by combining previously evolved building blocks (Lenski et al. 2003).

However, for representation of genetics within digital evolution various methods are interchangeably used. With Avida, the animal DNA is a computer algorithm, which directly represents executed behaviour. However this is not the case in natural organisms, as DNA describes the layout and physical structure of the body and brain, which in turn enables an individual to learn behaviour through their experience. In Avida certain commands are rewarded with increased computing power, again this method may not accurately represent methods within natural organisms.

Darwin Pond (2005) is an evolution simulator for 'Swimmers'. Food grows at a predefined growth and spread rate throughout the environment (Fig. 1). Swimmers have characteristics setting their hunger level, maximum lifespan, energy from food and energy from mating. Individual swimmers can be saved as .dna files which contain the genes, saved as around 16 ten digit numbers. Each swimmer is differentiated from others by individual settings for variables including: number of limbs, segments per limb, rate, amplitude, straddle, turning, joint angle, motion genes, base colour and colour shift. A swimmer may only mate with swimmers of the same colour.

Other evolution simulators include corewars, a game in which algorithms compete for the core system memory, which causes a survival of the fittest mechanism.

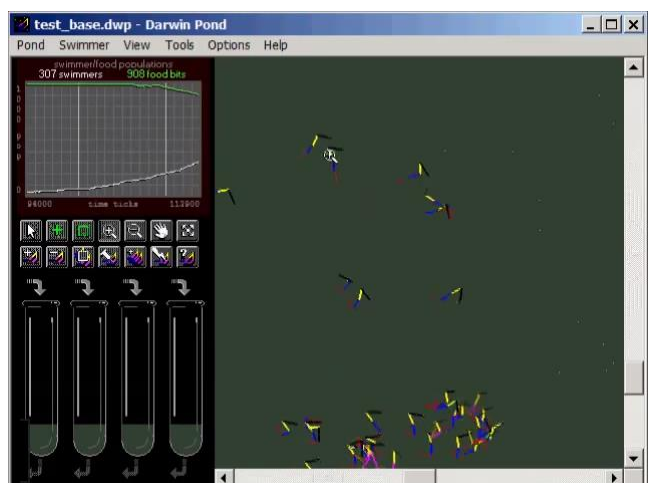


Fig. 1. Simulator of autonomous evolution in Darwin pond.

Physics Based Mobile Robot Simulators

There has been recent research focussing on 3D geometric model based creatures whose movement is governed by simulated laws of physics. Examples include artificial flying creatures created by modelling the air drag forces (Furukawa et al, 2010). Other virtual creatures have been able to use movement of their body parts, to drag themselves across a surface. Simulators may need to model several physical laws including gravity, momentum, energy transfer and others.

Evolution of group or co-operative mobility control and the co-ordination of movements has been a focus of recent research. These dynamics are critical to group behaviours such as flocking, avoiding obstacles, and eluding enemies.

Evolving motion strategies with a simulator could enable mobile robots to adapt to conditions in ways not otherwise apparent to human designers.

Recent studies suggest that when an evolving group is subjected to a catastrophic population bottleneck, the group often rebounds and that the result on average fitness and genetics can be comparable to the difference the system would have accumulated if it had been left untouched (Olson et al. 2013). Simulated robotic evolution may provide a method by which the effects of population rebounds on group genetics could be measured.

Results of Robot Motion Simulator

A simulator was developed to model autonomous robots which were mobile within a limited area on a flat surface.

The robotic agents were programmed to walk in random directions until food was within a certain distance (Fig. 2). Once food was seen the agents would walk towards the food and eat it. If the agents do not obtain food within a certain time the agents die and are removed from the simulation.

Breeding was implemented by genetic algorithms to enable the robotic agents to adapt in response to objects within the virtual environment. When breeding, each new robot's physical characteristics were based on their parents using crossover with random mutations. Physical characteristics include leg length and the distance of eyesight.

This system resulted in evolution of longer legs and better eyesight over time, due to survival of the fittest. A shortage of food eliminated the worst performing agents.

Finally when food quantity was increased to an amount where all agents could survive. When the amount of food was

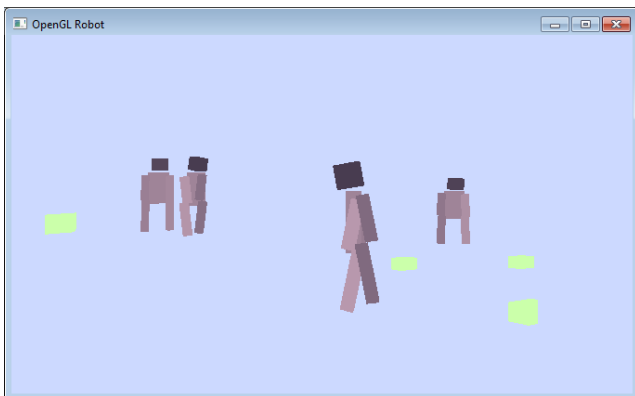


Fig. 2. Developed robot motion simulator.

increased, the survival of the fittest mechanism no longer occurred and average fitness stopped increasing over time since there was no longer a survival bottleneck. To assist the reader in visualising the simulator a short video was uploaded here: <https://www.youtube.com/watch?v=BNtT98MkYzM>

Discussion

The simulated evolution showed that increased fitness over time occurs only in the presence of survival bottlenecks, causing only the fittest to survive. In this simulation, the fittest robots with the fastest movement rate due to their larger leg components were more suited to reach food quickly and survive. When food was increased to a rate at which all robots were surviving, the fittest were no longer at an advantage.

Survival bottlenecks decimate the number of individuals in a species. Whilst many individuals suffer, the destruction can work in favour of the species as a whole, leaving the fittest and best adapted to survive. The average fitness will have increased. However when a species has access to more than enough food for all individuals, bottlenecks are eliminated. This enables the weakest individuals to survive with an equal chance of reproducing as the fittest and evolution stops.

This research has aimed to measure the effect of food bottleneck on the rate of evolution and average fitness.

Future evolution simulators may benefit from developing a standard method for storing and interpreting genetics as currently various methods are being used. In some cases genes represent physical characteristics, such as the number of limbs and limb length. Alternatively genes can executable code, representing behaviour as in Avida. In this case, the genes serve as an algorithm for behaviour which could include motion and logic based decision making.

Conclusions and Future Work

The next stage of research could be to implement computer vision for the autonomous agents. For each robot agent, the robotic field of vision can be calculated from the robot's position by projecting the view from their head, as 45 degree on the x and y axis. The resulting field of view can be calculated on each iteration of the software and used as input to computer vision algorithms. A variety of image processing algorithms can be applied. This may result in the robots evolving to respond to visual perceived colours, objects.

This could address a central problem to robotics, to appropriately respond to sensory information in real-time.

References

- Avida, Devosoft (2009), <http://avida.devosoft.org>.
- Bedau, M. A., Packard, N. H. (2003). Evolution of evolvability via adaptation of mutation rates. *Biosystems*, 69(2):143-162.
- Darwin Pond, Ventrella J, Dodd B (2005). <http://www.ventrella.com/darwin/darwin.html>.
- Furukawa, M., Morinaga, M., Watanbe, M., Suzuki, I., Yamamoto, M. (2010). Artificial flying creature by flapping. *IEEE International Conference on Systems Man and Cybernetics (SMC)*:624-629.
- Lenski R.E., (2003). The Evolutionary Origin of Complex Features. *Nature*, 423:139-144.
- Olson, R., Mirmomeni, M., Brom, T., Bruger, E., Hintze, A., Knoester, D., & Adami, C. (2013). Evolved digital ecosystems: Dynamic steady state, not optimal fixed point. *Advances in Artificial Life, ECAL*. 12:126-133.

Reaction-Diffusion Risk: Chemical Signaling in a Conquest Game

Nathanaël Aubert-Kato¹ & Olaf Witkowski²

¹Ochanomizu University, Tokyo

²The University of Tokyo, Tokyo

aubert.kato.nathanael@ocha.ac.jp, olaf@sacral.c.u-tokyo.ac.jp

Late-Breaking Abstract

The spontaneous generation of life has long been a central question investigated in the study of the origins of life [Szathmáry and Smith, 1995, Bedau et al., 2000]. The most common constructive approach to this problem might be artificial chemistry, the computer-inspired modeling of systems composed of chemical substances, either simulated with interaction rules and with more or less coarse-grained structures or implemented *in vitro*.

Reaction–diffusion (RD) systems, first introduced by Alan Turing [Turing, 1952], are models explaining how concentrations of spatially distributed chemical substances change locally with local reactions by which the chemicals are transformed into each other, and diffusion which causes the substances to spread out over a surface in space. One of the most famous artificial reaction diffusion system is the Belousov-Zhabotinsky chemical system, displaying complex temporal patterns [Zaikin and Zhabotinsky, 1970].

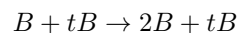
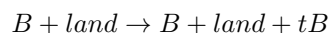
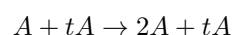
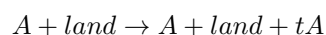
RD systems can be applied to molecular programming, involving the specification of structures, circuits and behaviors within living and non-living systems, in which decision-making will be carried out by chemical processes themselves.

In the past, RD-based molecular programming has been showing impressive results, both from the experimental side [Chirieleison et al., 2013, Padirac et al., 2013] and the theoretical side [Scalise and Schulman, 2014].

In this paper, we use a molecular programming model (implementing a Risk-like game¹-like simulation) to explore a minimalist type of signaling system, by which the state of an entity affects other entities. In particular, we explore the signaling between chemicals sub-

¹Risk is a strategy game, played on a board depicting a political map of the Earth, divided into forty-two territories. Players control armies with which they attempt to capture territories, with results determined by dice rolls. To win the game, object of the game is to occupy every territory on the board and in doing so, eliminate the other players.

stances within the following set of reactions, with interactions based on an extension of the system presented by Padirac et al. [2012] (Figure 1):



The "land" are chemical species that template the production of other species, which in turn is used to catalyze the production of signal. "Land" species are considered to be tethered to the surface and thus do not diffuse. They are also protected against degradation. All other species are degraded over time.

To allow for competition, the reactions based on substance A (resp. B) are inhibited by substance B (resp. A). Substances tA and tB represent "agents", whereas A and B are "signals". Signals can propagate much further than the agents themselves, and are used to take over new areas on the board. Population can also be neutral when as roughly as much A and B are present (including when they are both 0).

In simulation, a transient fight was observed (see Figure 2) between the agents tA and tB, for the conquest of a central land area. Interestingly, even at equilibrium, areas of influence were observed to be maintained by the exchange of signals A and B. In certain runs, because of the signaling-induced areas of influence, both agents were kept from some land area, which remained "neutral".

To wrap up, our preliminary results showed, for a simple reaction-diffusion molecular programming model, new insights on the influence of proto-signaling, as an indirect and delayed behavior that impacts on

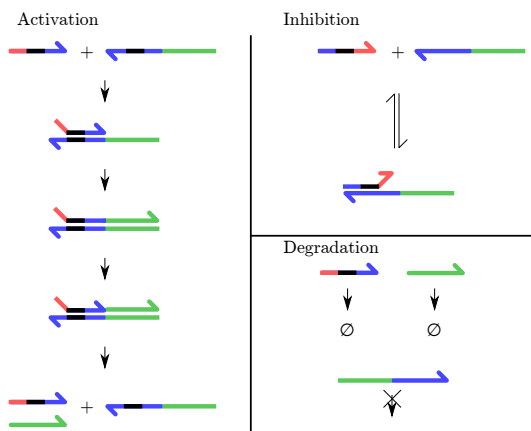


Figure 1: **Diagram of considered molecular programming reactions, displaying the three fundamental principles of the model: activation, inhibition and degradation.** Activation: a signal strand attaches to a template species, generating a new molecular species. Inhibition: A signal can inhibit templates based on its counterpart by partially attaching to it. No reaction ensues due to the mismatches. Black: part common to both signal species, used to ensure the basic stability of all complexes. Degradation: all generated species are degraded over time, except for "land" species, which are chemically protected.

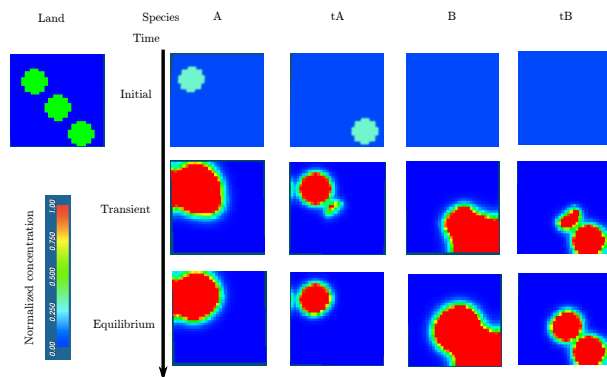


Figure 2: **Visualization of the different stages of a simulation.** Each square represents a local normalized heatmap of concentrations respectively in A, tA, B and tB, with values ranging from 0 (blue) to 1 (red). Simulated with Ready [Hutton et al.].

competition in multi-agent systems. In particular, it is interesting to notice the strong localization of "agents" in spite of the global catalysis from signal. While our approach relies on a DNA computing implementation for convenience, the principles of this study can be extended to various chemical systems. The next step will

consist in developing the model further with variation, to study the coevolution between signaling and heredity. It would be also interesting to implement stochasticity to have non-deterministic behaviors.

References

- Eörs Szathmáry and John Maynard Smith. The major evolutionary transitions. *Nature*, 374(6519):227–232, 1995.
- Mark A Bedau, John S McCaskill, Norman H Packard, Steen Rasmussen, Chris Adami, David G Green, Takashi Ikegami, Kuniyuki Kaneko, and Thomas S Ray. Open problems in artificial life. *Artificial life*, 6(4):363–376, 2000.
- Alan Mathison Turing. The chemical basis of morphogenesis. *Philosophical Transactions of the Royal Society of London B: Biological Sciences*, 237(641):37–72, 1952.
- AN Zaikin and AM Zhabotinsky. Concentration wave propagation in two-dimensional liquid-phase self-oscillating system. *Nature*, 225(5232):535–537, 1970.
- Steven M Chirieleison, Peter B Allen, Zack B Simpson, Andrew D Ellington, and Xi Chen. Pattern transformation with dna circuits. *Nature chemistry*, 5(12):1000–1005, 2013.
- Adrien Padiac, Alexandre Baccouche, Teruo Fujii, Andre Estevez-Torres, and Yannick Rondelez. Predator prey molecular landscapes. In *Advances in Artificial Life, ECAL*, volume 12, pages 791–792, 2013.
- Dominic Scalise and Rebecca Schulman. Designing modular reaction-diffusion programs for complex pattern formation. *Technology*, 2(01):55–66, 2014.
- Adrien Padiac, Teruo Fujii, and Yannick Rondelez. Bottom-up construction of in vitro switchable memories. *Proceedings of the National Academy of Sciences*, 109(47):E3212–E3220, 2012.
- Tim Hutton, Robert Munafo, Andrew Trevor-row, Tom Rokicki, and Dan Wills. Ready, a cross-platform implementation of various reaction-diffusion systems. URL <https://github.com/GollyGang/ready>.

Author Index

Aubert-Kato, Nathanaël, 29

Bilotta, Eleonora, 15
Borrego-Díaz, Joaquín, 4

Calisti, Marcello, 7
Corucci, Francesco, 7

Ellery, Alex, 12

Gómez Soto, José Manuel, 1
Galán-Páez, Juan, 4

Hashimoto, Yasuhiro, 17
Hauser, Helmut, 7
Hogeweg, P., 9
Husbands, Philip, 19

Ikegami, Takashi, 17

Johnson, Chris, 19

Laschi, Cecilia, 7
Lucente, Roberta, 15

Mediano, Pedro A.M., 22
Minoru, Asada, 25
Mori, Hiroki, 25

Oka, Mizuki, 17

Pantano, Pietro, 15
Park, Jihoon, 25
Philippides, Andrew, 19

Shanahan, Murray, 22
Swaid, Bashar, 15

van Dijk, B., 9
Vaughan, Neil, 27

Witkowski, Olaf, 29
Wuensche, Andrew, 1